Prediction of unusual stable ordered structures of Au-Pd alloys via a first-principles cluster expansion

Sergey V. Barabash,[1] Volker Blum,[1,*] Stefan Müller,[2] and Alex Zunger[1,†]
[1]*National Renewable Energy Laboratory, Golden, Colorado 80201, USA*
[2]*Universität Erlangen-Nürnberg, Germany*

(Received 24 September 2005; revised manuscript received 15 February 2006; published 13 July 2006)

We describe an iterative procedure which yields an accurate cluster expansion for Au-Pd using only a limited number of *ab initio* formation enthalpies. Our procedure addresses two problems: (a) given the local-density-approximation (LDA) formation energies for a fixed set of structures, it finds the pair and many-body cluster interactions best able to predict the formation energies of new structures, and (b) given such pair and many-body interactions, it augments the LDA set of "input structures" by identifying additional structures that carry most information not yet included in the "input." Neither step can be done by intuitive selection. Using methods including genetic algorithm and statistical analysis to iteratively solve these problems, we build a cluster expansion able to predict the formation enthalpy of an arbitrary fcc lattice configuration with precision comparable to that of *ab initio* calculations themselves. We also study possible competing non-fcc structures of Au-Pd, using the results of a "data mining" study. We then address the unresolved problem of bulk ordering in Au-Pd. Experimentally, the phase diagram of Au-Pd shows only a disordered solid solution. Even though the mixing enthalpy is negative, implying ordering, no ordered *bulk* phases have been detected. Thin film growth shows $L1_2$-ordered structures with composition Au_3Pd and $AuPd_3$ and $L1_0$ structure with composition AuPd. We find that (i) all the ground states of Au-Pd are fcc structures; (ii) the low-T ordered states of *bulk* Au-Pd are different from those observed experimentally in *thin* films; specifically, the ordered bulk Au_3Pd is stable in $D0_{23}$ structure and and AuPd in chalcopyritelike Au_2Pd_2 (201) superlattice structure, whereas thin films are seen in the $L1_2$ and $L1_0$ structures; (iii) $AuPd_3$ $L1_2$ is stable and does not phase separate, contrary to the suggestions of an earlier investigation; (iv) at compositions around Au_3Pd, we find several long-period superstructures (LPS's) to be stable, specifically, the one-dimensional LPS $D0_{23}$ at composition Au_3Pd and two two-dimensional LPS's at compositions $Au_{13}Pd_4$ and $Au_{11}Pd_4$; (v) Au-Pd has a number of unsuspected ground states, including the structure Au_7Pd_5 with the lowest formation enthalpy and the (301) "adaptive structures" in the Au-rich composition range, all of which could not be predicted by other theoretical methods.

DOI: 10.1103/PhysRevB.74.035108 PACS number(s): 61.66.Dk, 61.50.Ah, 81.05.Bx, 81.30.Bx

I. INTRODUCTION

Finding the most stable crystal structures of compounds is one of the classical problems in inorganic solid-state,[1,2] metallurgy,[3,4] and solid-state physics,[5–7] both because it represents the deepest and most stable aspect of our understanding of bonding and cohesion and because knowing the *structure* of perfect crystalline solids often holds the key to materials *properties*. Within the realm of intermetallic systems, much effort has been invested in theoretical predictions of structure.[6–11] A particularly hard problem is understanding of the structures spanned by compounds of Pd with Cu, Ag, or Au. Even though all four elements have complete electronic *d* shells and are thus not expected, by common metallurgical wisdom,[4] to form ordered compounds, they do form a fascinating diversity, as illustrated by their 50%-50% structures: CuPd has the bcc CsCl-type structure and AgPd is predicted to have a trigonal $L1_1$ structure [that is, a Ag_1Pd_1 (111) superlattice],[12–14] whereas AuPd is predicted[15] to have a chalcopyritelike Au_2Pd_2 (201) superlattice structure (referred to as "CH"[16]). Indeed, whereas the stable phases of Cu-Pd are known experimentally,[17] those of Ag-Pd and Au-Pd are not. For example, whereas the measured mixing enthalpy[18] of $Au_{1-x}Pd_x$ is negative at all x (implying that the system must order at low temperatures[19]), long-range order has not been observed experimentally in bulk $Au_{1-x}Pd_x$. Thin film studies found structures with (001) type order—i.e., $L1_2$ type around compositions $Au_{0.75}Pd_{0.25}$ and $Au_{0.25}Pd_{0.75}$,[20,21] and $L1_0$-type[22] around $Au_{0.5}Pd_{0.5}$, in contradiction to the theoretical prediction for bulk AuPd.[15] However, it is not clear whether the ordering observed in thin films is a result of the kinetics being faster than in bulk (in which case, the bulk could have similar structures) or the thin film ordering is qualitatively different (in which case these ordered phases may not appear in bulk). Indeed, thin films of various materials are known to exhibit long-range order of a different type than the bulk samples of the same material, as has been demonstrated both experimentally and theoretically (see, e.g., Refs. 23–26). Finding what are the stable bulk structures of Au-Pd is a challenge that we would like to address.

Even more intriguing than these structures is the occurrence of "natural long-period superstructures" based on the $L1_2$ building block in such systems. Indeed, a long-standing problem in metallurgy[10,27–29] has been the competition between the members of the family of $L1_2$-based superstructures. Experimentally, fcc alloys such as Cu-Pd with composition around A_3B and AB_3 frequently order into either the $L1_2$ structure or one of the related superstructures formed by introducing "antiphase boundaries" [usually (100) planes] separating the $L1_2$ domains shifted by $(0,\frac{1}{2},\frac{1}{2})$ [Fig. 1(a)]. The resulting long-period superstructures (LPS's) are distinguished by the distance M between two such boundaries. The most common LPS's in this family are $L1_2$ ($M=\infty$), $D0_{22}$ ($M=1$), and $D0_{23}$ ($M=2$) [Figs. 1(b)–1(d)], but many other

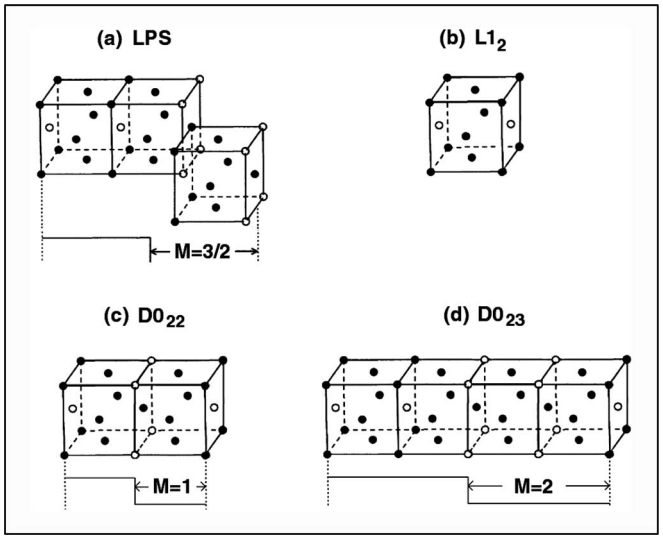

FIG. 1. Schematic of several $L1_2$-based long-period superstructures (LPS's). Generally, an LPS (a) can be constructed from an $L1_2$ unit (b) by modulating it with a square wave. An antiphase boundary is introduced whenever the modulation function changes sign, and the structure is denoted by specifying the length of nonantiphased domains in the unit cell. The LPS shown in panel (a) has modulation wavelength $M=\frac{3}{2}$ (in units of the fcc lattice parameter) and fundamental reciprocal-space wave vector $\mathbf{k}=\langle 1\frac{1}{2M}0\rangle=\langle 1\frac{1}{3}0\rangle$. Some common alloy ground states are, in fact, LPS's, including (b) $L1_2$ itself ($M=\infty$), (c) $D0_{22}$ ($M=1$), and (d) $D0_{23}$ ($M=2$).

long-period superstructures (including two-dimensional LPS's in which the antiphase modulation occurs simultaneously in two directions) have been observed in a number of intermetallic systems such as Cu-Pd, Au-Mn, Al-Ti, Au-Cd, Au-Zn, etc.,[30–35] but no LPS's have been seen in the bulk Au-Pd system. Local-density-approximation (LDA) calculations for $L1_2$, $D0_{22}$, and $D0_{23}$ structures of Au-Pd and Cu-Pd are summarized in Fig. 2 and illustrate the subtlety of the energetics of long-period superstructures in such systems. For example, (i) the *order* of A_3B vs AB_3 structural energies is different in both Cu-Pd and Au-Pd systems. As we will see below, this means that odd-body (three and above) interatomic interactions must be present. (ii) The energy of $D0_{23}$ is different from the average energy of $L1_2+D0_{22}$ (dotted lines in Fig. 2) for all cases. As we will see below, this means that interatomic interactions ranging to at least the eighth nearest neighbor must be present.[37] (iii) Finally, the difference between the energy of $D0_{23}$ and the average energy of $L1_2$ and $D0_{22}$ (δ in Fig. 2) has different signs in Au_3Pd and $AuPd_3$.[36] As we will see below, this means that *odd-body* (three and above) interatomic interactions ranging to at least the *eighth nearest neighbor* must be present. Clearly, determining the sequence of structural stability in LPS is a subtle problem.

A large group of theoretical methods which aim at predicting stable structures explores only those structures whose energy can be calculated directly—often a rather restricted set of candidate structures. For example, traditional total energy E_{tot} vs volume calculations[12,13,38–42] select the lowest E_{tot} from a small, preselected set of $\mathcal{O}(10)$ structures; the potential for missing ground states is rather large. The Connolly-Williams[43] approach applied in Refs. 44–46 involves the calculation of the total energies of $\mathcal{O}(5)$ structures, extracting from those $\mathcal{O}(5)$ interatomic interactions (typically up to the nearest neighbors), but applying those to analyze the stability of only the same $\mathcal{O}(5)$ input structures. For Au-Pd, such an investigation has been conducted by Mohri *et al.*,[46] with Au_3Pd $L1_2$, AuPd $L1_0$, and AuPd3 $L1_2$ assumed to be the ground states.

Theoretical studies employing the generalized perturbation method or the embedded-cluster method together with coherent potential approximation[47–49] can estimate interactions beyond the nearest neighbors. Those interactions could, in principle, be used to examine the energies of many other candidates. In practice, however, the library of tested struc-

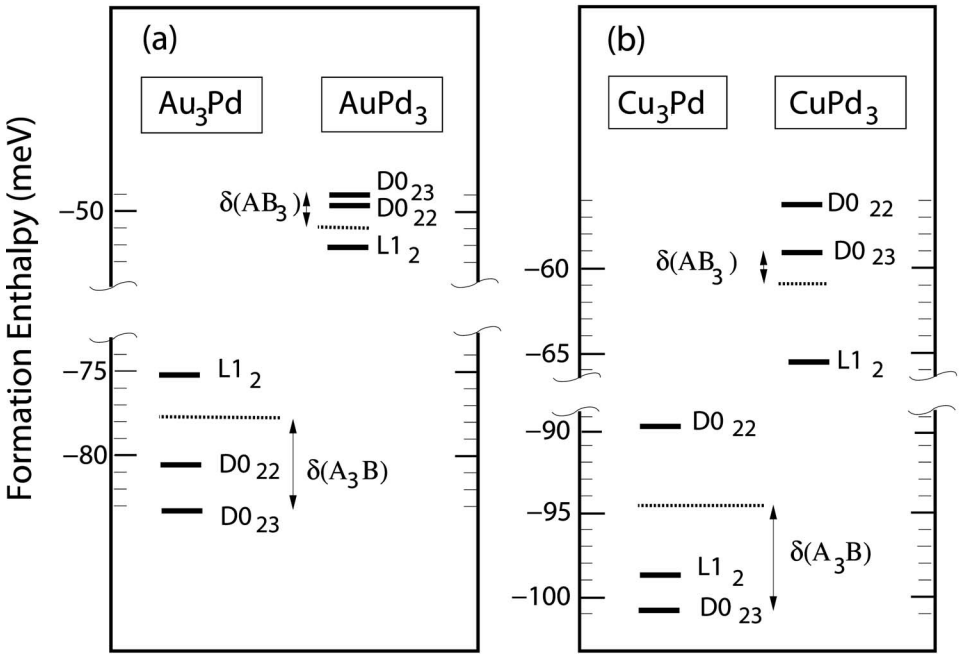

FIG. 2. The energetic order of $L1_2$, $D0_{22}$, and $D0_{23}$, at compositions A_3B and AB_3, as given by the LDA calculations for (a) Au-Pd and (b) Cu-Pd. The thick horizontal lines indicate the formation enthalpies of individual compounds, and the dashed lines indicate the average formation enthalpy of $L1_2$ and $D0_{22}$ structures, $[\Delta H(L1_2)+\Delta H(D0_{22})]/2$. The vertical arrows indicate the actual difference δ between $\Delta H(D0_{23})$ and the average $[\Delta H(L1_2)+\Delta H(D0_{22})]/2$. To properly account for this difference, CE needs to include interactions reaching to at least the eighth coordination shell.

tures is again often limited to $\mathcal{O}(10)$ structures (see, e.g., Refs. 50–52). For example, for the case of Au-Pd, Weinberger *et al.*[50] calculated pair interactions up to the fifth nearest neighbor, but used only the shortest two to select the most stable among those eight structures described by an exactly solvable model.[8] Still, that analysis yielded results different from the simple Connolly-Williams study, suggesting that Au_3Pd would order into $D0_{22}$, not $L1_2$.

A somewhat larger library of structures is considered by the "data mining" technique employed in Refs. 15 and 53. In this approach, correlations are sought among the calculated total energies for $\mathcal{O}(200)$ structures of $\mathcal{O}(100)$ A-B systems, so that one could guess by doing *fewer* than 200 calculations what is the likely structure of a new system A'-B' not in the database. On this basis, Curtarolo *et al.*[15] predicted that (i) Au_3Pd would order into $D0_{23}$ (which they find to be lower in energy than both $D0_{22}$ and $L1_2$) and that AuPd would order into the CH structure (the former conclusion contradicts the suggestions of Ref. 50, while the latter is consistent with them), that (ii) $Au_{0.75}Pd_{0.25}$ might not order but rather phase separate at low temperatures into AuPd CH and fcc Pd, and that (iii) $Au_{0.67}Pd_{0.33}$ would order into the $C37$ structure, which is a non-fcc structure.

The disagreement between the earlier theoretical studies of Au-Pd demonstrates that one cannot *guess* at the outset a set of select structures from which ground states can be selected. Instead, one should investigate a reasonably large portion of the structural phase space. If only the few simplest interactions (e.g., only the nearest and next-nearest pair interactions) were sufficient to describe the alloy energetics, one could use analytic methods[8,54–59] to investigate the full fcc phase space. Unfortunately, the complexity of interactions in realistic alloys may greatly exceed the capabilities of those analytic methods. This is particularly so for Au-Pd system, in which the LPS energetics requires the presence of long-ranged many-body interactions (see Sec. IV).

The implications of this complexity for a first-principles study are twofold. First, we need efficient methods to distill the important interactions, given that LDA formation energies can be calculated only for a subset of all possible configurations. Second, given those interactions, we need to explicitly search over a large a portion of the phase space to identify the ground-state structures. (In fact, we rigorously[60] find all the ground states with up to a given number N of atoms per cell, predicted by a particular set of interatomic interactions.)

In the present work, we study Au-Pd using the mixed basis cluster expansion (MBCE) method[6,61] in which we map a set of LDA total energies of N_s structures $[\mathcal{O}(50)]$ onto a generalized Ising Hamiltonian whose pair and many-body interactions are selected solely based on the ability to accurately *predict* LDA total energies of structures not included in the input set. The selection of the many-body terms is done via a genetic algorithm.[62] Our procedure iteratively solves two problems: (a) given the LDA formation energies for a fixed set of structures, it finds the pair and many-body cluster interactions best able to predict the formation energies of new structures, and (b) given such pair and many-body interactions, it augments the LDA set of "input structures" by identifying additional structures that carry most information not yet included in the "input." Our method provides controlled high accuracy (approaching the accuracy of the LDA), accounting fully for atomic relaxation effects, and allowing one to scan $\mathcal{O}(10^6)$ structures in a search for the true ground states. Our approach also results in a cluster expansion that can be used to predict finite-temperature quantities such as order-disorder transitions T_{ord} and short-range order at $T > T_{ord}$. However, our study is limited by the assumption of the exclusion of non-fcc structures. We will justify this assumption *ex post facto* by calculating via the LDA the energies of the non-fcc structures suggested as candidate stable structures in data mining calculations[15] and comparing them to the LDA energies of the fcc ground-state structures identified in our study.

The main findings for the Au-Pd system are (i) all the ground states of Au-Pd are fcc structures; (ii) the predicted low-T ordered states of bulk Au-Pd are different from those observed in thin films; specifically, the predicted ordered states of bulk Au_3Pd and AuPd are $D0_{23}$ and CH, respectively, whose energies are found to be lower than the (bulk) energies of the structures seen in thin films ($L1_2$ and $L1_0$, respectively) by almost 10 meV per atom; (iii) $AuPd_3$ $L1_2$ is stable and does not phase separate; (iv) at compositions around $x \sim 1/4$, several one- and two-dimensional long-period superstructures are stable at low T; (v) there are a number of completely unsuspected ground states (including the structure Au_7Pd_5 with the lowest formation enthalpy), all of which could not be predicted by other theoretical methods.

The rest of the paper is organized as follows. In Sec. II we describe our methodology, beginning with the general formulation of the cluster expansion formalism and then describing the two loops of the iterative procedure that we use to construct a highly accurate cluster expansion. In Sec. III we discuss the calculation of the input formation enthalpy ΔH_{LDA} values, and in Sec. IV we discuss the consequences of the observed LDA hierarchy of LPS for the range of interactions needed to describe Au-Pd. Section V illustrates how the procedures set forth in previous sections are implemented in the case of Au-Pd. We demonstrate the accurate predictive power of the resulting cluster expansion in Sec. VI. Finally, in Sec. VII we analyze the ordered states at $T=0$ predicted by our final cluster expansion.

II. METHODOLOGY

A. General formulation of the cluster expansion

A configuration σ is defined as an occupation pattern of the $i=1,\ldots,N$ fcc lattice sites by Au or Pd. We assign a pseudospin variable $S_i=-1$ to the site i if that site is occupied by Au and $S_i=+1$ if it is occupied by Pd. We wish to predict from first principles the $T=0$ stable structures in the Au-Pd system by scanning a much larger library of possible structures (in practice, $\sim 1\,500\,000$) than is practical to calculate explicitly via the LDA. Since it is tedious to calculate more than, say, ~ 100 total energies, we aim at finding a cluster expansion[63] $\Delta H_{CE}(\sigma)$ able to predict the directly calculated formation enthalpy

$$\Delta H_{LDA}(\sigma) \equiv E_{tot}(\sigma, V_\sigma, \{\mathbf{R}_{relaxed}\}) - (1-x_\sigma)E_{tot}(Au, V_{Au}) - x_\sigma E_{tot}(Pd, V_{Pd}) \quad (1)$$

with the accuracy of a few meV. Here, x_σ is the Pd composition, and V_σ, V_{Au}, and V_{Pd} are the equilibrium molar volumes of the structure σ and the pure elements, respectively. The relaxation $\{\mathbf{R}_{relaxed}\}$ involves both minimization of $E_{tot}(\sigma)$ with respect to unit cell vectors ("cell external"[61] parameters yielding V_σ) and with respect to atomic positions within the cell ("cell internal"[61] parameters).

For compounds made of lattice-mismatched constituents (say, $V_A > V_B$), a piece of $\Delta H(\sigma)$ originates from strain. For example, if σ is an A_nB_m-layered structure made of n layers of A and m layers of B along direction $\hat{G}$, there is a "constituent strain" energy $E_{CS}(\hat{G})$ corresponding to compressing material A in the $\hat{G}$ plane and expanding material B in the $\hat{G}$ plane (thereby achieving a common in-plane lattice parameter $a_\perp^{eq}$ for A and B layers). Expansion of this energy in pair interactions requires long-range interactions, and thus the constituent strain energy $E_{CS}(\sigma)$ is subtracted from $\Delta H_{LDA}(\sigma)$,[61] so we expand only the difference $\Delta\tilde{H}_{LDA} = \Delta H_{LDA} - E_{CS}(\sigma)$. To find $E_{CS}(\sigma)$ for a general configuration σ, we first use *ab initio* data to find the epitaxial strain energies $\Delta E_\iota^{epi}(\hat{G}, a_\perp^{eq}) \equiv E_\iota(a_\iota) - E_\iota^{epi}(\hat{G}, a_\perp^{eq})$ of pure periodic element ι ($\iota = A$ or B) deformed along direction $\hat{G}$ in such a way that the in-plane lattice constant is given by $a_\perp^{eq}$. [The appropriate composition-dependent $a_\perp^{eq}$ is in turn determined self-consistently from $\Delta E_A^{epi}(\hat{G}, a)$, as discussed in Ref. 64.] We then define

$$E_{CS}(\sigma) = \sum_{\mathbf{G}\neq 0} [(1-x)\Delta E_A^{epi}(\hat{G}, a_\perp^{eq}) + x\Delta E_B^{epi}(\hat{G}, a_\perp^{eq})] \times |S(\mathbf{G}, \sigma)|^2 F(\mathbf{G}), \quad (2)$$

where $S(\mathbf{G}, \sigma) = 1/N\Sigma_i S_i(\sigma) e^{i\mathbf{G}\cdot\mathbf{R}_i}$ and we use the attenuated constituent strain[65] with $F(\mathbf{G}) = \exp[-(|\mathbf{G}|/k_c)^2]$ (where $k_c = 2\pi/a$).

We expand the relative formation enthalpy $\Delta H_{LDA} - E_{CS}(\sigma)$ of an arbitrary binary structure as

$$\Delta\tilde{H}_{CE}(\sigma) = J_0 + \sum_i J_i S_i(\sigma) + \sum_{j<i} J_{ij} S_i(\sigma) S_j(\sigma) + \sum_{k<j<i} J_{ijk} S_i(\sigma) S_j(\sigma) S_k(\sigma) + \cdots, \quad (3)$$

where $J_0, \{J_i\}, \{J_{ij}\}, \ldots$ are the coefficients that need to be determined. Introducing inequivalent "many-body interaction types" (MBIT's)—i.e., various combinations of three, four, etc., points on the underlying fcc lattice, we can define space-averaged pseudospin product corresponding to a given MBIT f in configuration σ:

$$\bar{\Pi}_f(\sigma) = \frac{1}{ND_{f(i_1,i_2,\ldots,i_m)\sim f}} \sum S_{i_1}(\sigma) S_{i_2}(\sigma) \cdots S_{i_m}(\sigma), \quad (4)$$

where the sum runs over the ND_f instances of the MBIT f.[60] Then Eq. (3) can be rewritten as

$$\Delta\tilde{H}_{CE}(\sigma) = J_0 + (2x-1)J_1 + \sum_{\text{pairs}}^{n_{\text{pairs}}} D_{\text{pair}} J_{\text{pair}} \bar{\Pi}_{\text{pair}}(\sigma) + \sum_f^{N_{MB}} D_f J_f \bar{\Pi}_f(\sigma), \quad (5)$$

where again J_0, J_1, $\{J_{ij}\}$, and $\{J_f\}$ are coefficients that need to be determined. While the number of terms needed to make the mapping of Eq. (5) exact is 2^N [thus, both the determination of J's and calculation of $\Delta H_{LDA}(\sigma)$ for all 2^N structures σ are difficult], in practice some interactions are more important than others, and a truncated series may still give a good approximation to $\Delta H_{LDA}(\sigma)$. We thus need to select which pairs and which MBIT's are to be kept in the truncated expansion. This should be done in such a way that the resulting cluster expansion has real *predictive* power, besides simply fitting well the input ΔH_{LDA}'s.

B. Flowchart of the cluster expansion procedure

Our strategy to identify the most important terms in Eq. (5) consists of two "loops," as visualized in Fig. 3. The goal of the inner loop is to identify, for a fixed set of N_s input structures, the set of pairs and many-body interactions with the best ability to predict structures which were not included in the fit. The "outer loop" iteratively adds new ground-state candidate structures predicted by the cluster interactions found in the inner loop. The "outer loop" thus acts as a feedback loop against spurious ground-state predictions from the inner loop and/or artifact interactions found on the basis of too few input structures. We next explain the two loops in more detail.

C. Inner loop and cross-validation

At each outer loop iteration i we provide the inner loop with an input set of $N_s^{(i)}$ structures (see Fig. 3). To calculate the predictive power of different truncated cluster expansions ("CE candidates") for this input set, we break (Fig. 3) the set of $N_s^{(i)}$ structures into two subsets: the set used to fit $\{J\}$ ("fitting set") made of $N_f^{(i)}$ structures and a nonoverlapping set of $N_v^{(i)} = N_s^{(i)} - N_f^{(i)}$ structures reserved for testing predictions ("prediction set"). By subdividing the input set into the prediction set and fitting the set in different ways we create $b^{(i)}$ prediction sets. We will generate a few cluster expansions for each outer-loop iteration i. The quality of the νth CE (CE_ν) is obtained by comparing its predictions to the directly calculated LDA energies of the $N_v^{(i)}$ structures left out during fitting and averaging the errors over all $b^{(i)}$ prediction sets. This gives the "*leave-many-out cross-validation*" (CV) score:

$$S_{CV}^i(\text{CE}_\nu) = \frac{1}{b^{(i)} N_v^{(i)}} \sum_{b^{(i)}\text{sets}} \sum_{\sigma=1}^{N_v^{(i)}} |\Delta\tilde{H}_{CE}^{(i,\nu)}(\sigma) - \Delta\tilde{H}_{LDA}(\sigma)|^2. \quad (6)$$

We set $N_v^{(i)}$ to roughly a third of the total input size $N_s^{(i)}$.

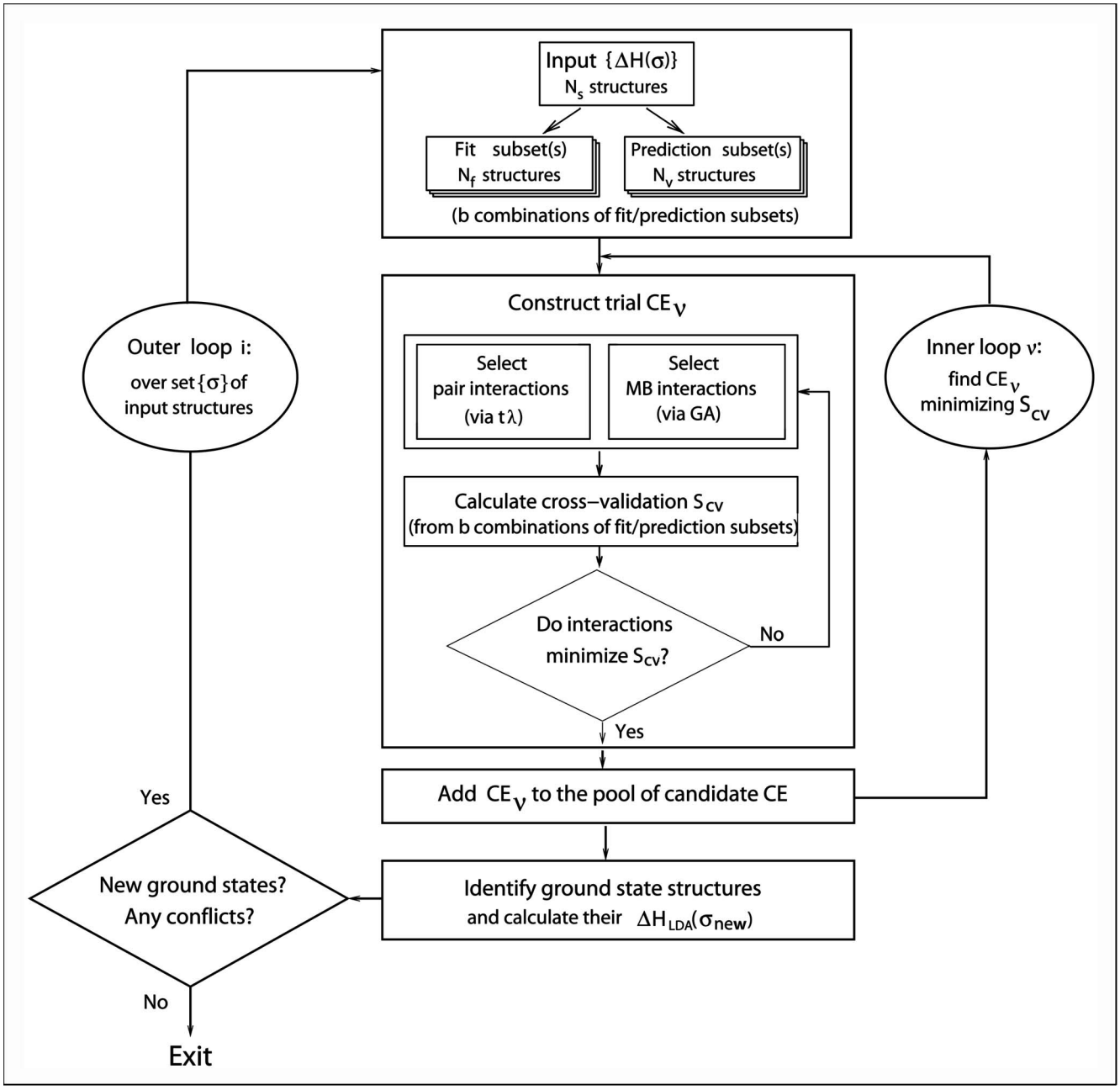

FIG. 3. Flowchart of the iterative procedure that we use to establish our cluster expansion.

While it is numerically prohibitive to use all $\binom{N_v^{(i)}}{N_s^{(i)}}$ possible prediction sets, we can choose the prediction sets and the value of $b^{(i)}$ in such a way that each structure enters at least two prediction sets. The choice of the prediction sets is kept constant throughout the given outer loop iteration. For a discussion of the advantages of leave-many-out CV over alternative schemes the reader is referred to Refs. 66 and 67.

In the inner loop, one needs to select which pairs and which MBIT's best represent $\{\Delta H_{LDA}(\sigma)\}$. It is convenient to treat separately pairs and MBIT's. The *pair coefficients* J_{ij} are determined using the "t-λ" constrained fit,[61] which allows us to keep, in principle, an infinite number of pair terms.[61] For that, we rewrite the sum over pairs, Eq. (5), as

$$\sum_{\text{pairs}}^{n_{\text{pairs}}} D_{ij} J_{ij} \bar{\Pi}_{\text{pair}}(\sigma) = \sum_{\mathbf{k}} J(\mathbf{k}) |S(\mathbf{k},\sigma)|^2, \tag{7}$$

where the sum is over a *finite* number of reciprocal-space $\mathbf{k}$ vectors in the Brillouin zone for which $S(\mathbf{k},\sigma)$ is nonzero. The pair coefficients are then the values determined by minimizing

$$s_{MBCE} = \sum_{\sigma \notin \text{pred.set}} |\Delta \tilde{H}_{LDA}(\sigma) - \Delta \tilde{H}_{CE}(\sigma)|^2 + tM, \tag{8}$$

where

$$M = \frac{1}{\alpha}\sum_{\mathbf{k}} J(\mathbf{k})[-\nabla_{\mathbf{k}}^2]^{\lambda/2} J(\mathbf{k}) = \sum_{ij}^{n_{\text{pairs}}} R_{ij}^{\lambda} D_{ij} J_{ij}^2 \qquad (9)$$

and the sum in Eq. (8) runs over the structures not belonging to the prediction set. Here t is a Lagrangian multiplier and α a normalization factor. The role of the additional term tM is to enforce the spatial decay of J_{ij} with the pair distance R_{ij}, allowing only those pair interactions that improve the fit. We asses different values of t, λ, and n_{pairs} by means of CV score and find the optimal $\{t, \lambda, n_{\text{pairs}}\}$ values for each given combination of MBIT's.

We determine the *many-body* interactions in the inner loop by using a genetic algorithm (GA).[62] To do so we construct a large pool of all MBIT types up to a given order.[68–70] This pool includes over 100 MBIT's—i.e., many more than we will need (we will end up using only 7 MBIT's in our final CE). Then we impose a restriction that no more than N_{MB} MBIT's may be nonzero in the final CE fit. The optimum combination of the nonzero MBIT interactions is then found by the GA, using the procedure established in Ref. 62. In that procedure, a "population" consisting of N_{pop} CE "individuals" is evolved over a number of "generations," with "mating," "mutation," and "adjustment" steps (as described in Ref. 62) performed at each generation to replace the $(1-r_s)N_{pop}$ "least-fit" CE individuals (those having the highest S_{CV}) by new, possibly better individuals. The GA performance has been found not to depend strongly on the population size N_{pop} and on the "survival rate" r_s, but to be sensitive to the "mutation rate" and to the use of "lock-out" strategy which brings the GA out of deep local minima in the search space.[62] We use the GA parameters established in Ref. 62, including the average "mutation rate" of two mutations per new individual and "lock-out" after ~100 locked-in generations.

There is a certain risk of CV overoptimization[66,67,71]—that is, of finding combinations of MBIT's which happen to have a low CV score only because the amount of LDA data used for CV was limited. Overoptimized CE candidates are eliminated in the outer loop, where we analyze the predictions of *several* CE candidates to minimize the influence of possible CV overoptimization. At each iteration i, we determine the number N_{MB}^{opt} of MBIT's sufficient to achieve a low CV score and select several best CE candidates with $(N_{MB}^{opt}-2)\cdots N_{MB}^{opt}$ MBIT's. We then analyze the predicted energetics and, particularly, the predicted ground states of those candidates. This allows us to first consider *typical* (frequent) ground-state predictions.[72] Furthermore, we minimize the probability of CV overoptimization by restricting the *number* N_{MB} of MBIT's by the value N_{MB}^{opt} that provides low, but not necessarily minimal, CV scores. This ensures the "redundancy" of the input data used for fitting, resulting in more reliable predictions. Nonetheless, a slight bias from a finite CV score can never be excluded. This is precisely why we need the outer loop: if we ever by accident find an artifact result from a badly chosen inner-loop iteration, the outer loop will catch it.

D. Outer loop and the ground-state search

We are now in a position to test how well the predictive accuracy of our cluster expansion extends to the structures outside the set of $N_s^{(i)}$ input structures. In particular, we want to ensure that the ground states predicted by the cluster expansion are all in agreement with the LDA. This is done in the outer loop, which adds the structures to the input set and examines the predictivity as the set of input structures is varied. We view the outer loop of CE as an engine that helps us navigate in the space of structures, directing us to those that merit LDA calculations. Our "input set" thus eventually includes all the ground-state structures; in addition, it includes other structures needed to give the CE a prediction ability over the entire structural phase space, including the structures with energies much higher than energies of the ground states. Note that the role of the outer loop is only to vary the set of the input structures; the interactions of Eq. (5) are all found in the inner loop.

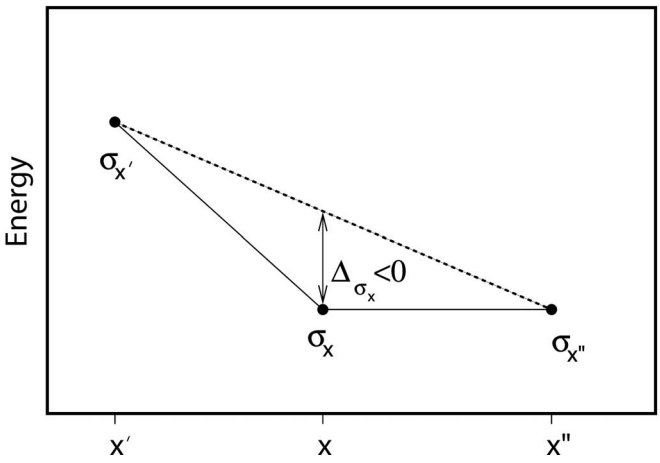

FIG. 4. Schematic illustration of convex hull construction during a ground-state search. In order to be stable with respect to disproportionation into structures at concentrations x' and x'', a ground-state structure σ_x at concentration x must lie below the "tie-line" connecting $\sigma_{x'}$ and $\sigma_{x''}$.

At the end of a given inner-loop iteration, we have selected several CE candidates constructed from a *given* set of input structures. To decide which new structures now need to be tested in the LDA for the next iteration of the outer loop, we perform a ground-state search for each of the selected CE candidates by calculating $\Delta H_{CE}(\sigma)$ for all possible structures σ up to $N=20$ atoms per unit cell. This is done in two steps: First, at each concentration x (among the finite number of concentrations possible in such finite-size structures), we find the structure σ_x with the lowest $\Delta H_{CE}(\sigma_x)$. Not all such structures are yet ground states, for some may be unstable with respect to disproportionation into structures $\sigma_{x'}$ and $\sigma_{x''}$ at some other concentrations x' and x'' (Fig. 4). Second, we build a convex hull[8] consisting of only those structures σ_x that lie below the "tie-line" connecting any other two structures. This convex hull forms our predicted ground-state line, from which we select new input structures for the next outer-loop iteration. Since such a "direct enumeration"[16] approach evaluates *all* possible structures up to N atoms per cell, it can be realistically done only for $N \sim 20$ atoms ($\sim 10^6$ structures) even if we use a simple expression like ΔH_{CE} of Eq. (5). For practicality reasons, we further restrict the search during the first few outer-loop iterations by searching only up to $N=16$ atoms per cell.

Our criteria for selecting the structures to serve as new inputs at the next outer-loop iteration are based on the frequency of occurrence of a given structure in predictions of different CE's and on the predicted energetic depth of the ground-state structure. We define the depth Δ_j^ν of a ground state j (at concentration x_j) with respect to the tie-line of the neighboring ground states $j-1$ and $j+1$ of the *same* CE candidate CE_ν:

$$\Delta_j^\nu = \Delta H_{CE,j} - \left[\frac{(x_j - x_{j-1})}{x_{j+1} - x_{j-1}} \Delta H_{CE,j+1} + \frac{(x_{j+1} - x_j)}{x_{j+1} - x_{j-1}} \Delta H_{CE,j-1} \right]. \tag{10}$$

We use Δ_j^ν as a measure of importance of a ground-state prediction for a given CE_ν.

We use the following criteria to select the structures to be calculated *ab initio* and added to the input of the next outer loop iteration: (i) deep frequent predictions, (ii) deep infrequent predictions if the structure is not very large, (iii) shallow frequent predictions if the structure is not very large, and (iv) untested predictions that persist through several iterations. Here, "deep" predictions are those with $\Delta_j < -1$ meV, "frequent" predictions are those predicted by more than 30% of CE candidates, and the "very large" structures are those that have more than eight atoms per primitive cell. The reasons for adopting such criteria are that we want to capture deep ground states early in the outer-loop iterations (besides, we tend to trust the LDA for deep-energy predictions more than for shallow-energy predictions) and that, if many CE candidates point to the same structure as a ground state, we want to keep such a structure for further outer-loop tests.

Last, in the final few iterations, we add ΔH_{LDA} values for structures whose predicted ΔH_{CE} are very different for different CE candidates, even if those structures are not close to the ground-state line. This helps to ensure that a final CE fit has good predictive power for any arbitrary structure.

The outer loop of the iterative CE search (Fig. 3) is terminated if all of the following conditions are met: (a) there are no new *deep* ground state predictions, (b) the predictions of different CE candidates for *all* structures up to 20 atoms per cell do not differ drastically (no more than by a few times the CV score), and (c) once we calculate the LDA values for some new structures (remaining shallow ground-state predictions or structures for which ΔH_{CE} differ most for different CE's), they reasonably agree with the predicted ΔH_{CE} range. When all these criteria are satisfied, we select as the final CE that one that gives the best description of the low-energy structures calculated in the LDA and use it for a final ground-state search.

III. CALCULATING $\Delta H_{LDA}(\sigma)$ FOR INPUT STRUCTURES

We calculated the ΔH_{LDA} values using the local-density approximation[73] to the density-functional theory.[74] We utilize ultrasoft pseudopotentials[75] and the plane wave basis set as implemented in the Vienna *ab initio* simulation package (VASP).[76,77] For a few key compounds, we have also compared the pseudopotential VASP calculations to full-potential all-electron LAPW results obtained with the WIEN2K package.[78] The differences in pseudopotential and LAPW results for the lattice parameters and for the bulk moduli was correspondingly 0.4% and 5% in both elemental Au and elemental Pd (as determined by fitting to the Murnaghan equation of state[79]), and the differences in formation enthalpies for compounds ($L1_0$, CH, Au_3Pd, and $AuPd_3$ $L1_2$) was less than 1.5 meV/atom.[80]

TABLE I. LDA formation enthalpies ΔH_{LDA} (in meV) of $Au_{1-x}Pd_x$ compounds used as the input to the first iteration of the outer-cluster expansion loop. Also shown the fitted ΔH_{CE} of the final CE.

x	Structure	Description	ΔH_{LDA}	Final ΔH_{CE}
0	$A1$	fcc Au	0.0	0.7
1/8	$D7a$		−40.5	−38.9
1/4	$Z1$	(100) A_3B SL	−59.3	−57.9
	$W1$	(311) A_3B SL	−65.7	−66.8
	$Y1$	(110) or (301) A_3B SL	−69.0	−68.7
	$L1_2$	not a SL	−75.1	−74.3
	$D0_{22}$	(201) A_3B SL	−80.5	−81.9
	$D0_{23}$	(401) A_5BAB SL	−83.3	−82.0
1/3	$\alpha 1$	(111) A_2B SL	−54.8	−54.8
	$\beta 1$	(100) or (301) A_2B SL	−77.1	−78.4
	$\gamma 1$	(110) or (201) A_2B SL	−87.8	−88.0
1/2	$Z2$	(100) A_2B_2 SL	−48.1	−48.6
	$L1_1$	(111) AB SL	−62.9	−63.2
	$Y2$	(110) A_2B_2 SL	−66.8	−66.4
	$W2$	(201) A_2B_2 SL	−75.6	−74.8
	$L1_0$	(100) or (201) AB SL	−82.0	−84.3
	CH	(201) A_2B_2 SL	−92.6	−90.0
2/3	$\alpha 2$	(111) AB_2 SL	−28.4	−28.3
	$\beta 2$	(100) AB_2 SL	−46.1	−44.6
	$\gamma 2$	(110) AB_2 SL	−53.0	−53.4
3/4	$Z3$	(100) AB_3 SL	−32.1	−32.3
	$Y3$	(110) AB_3 SL	−36.0	−35.9
	$W3$	(311) AB_3 SL	−36.2	−36.1
	$D0_{23}$	(401) AB_5AB SL	−49.0	−47.8
	$D0_{22}$	(201) AB_3 SL	−49.7	−49.9
	$L1_2$	not a SL	−52.2	−51.7
7/8	$D7b$		−19.1	−18.6
1	$A1$	fcc Pd	0.0	0.0

The LDA inputs ΔH_{LDA} to the first outer-loop iteration are listed in Table I. We begin with the formation enthalpies of 28 structures, which are not necessarily low-energy structures. This set is obtained by taking simple superlattices in major directions, to which we add some common ordered fcc structures. Table II lists the ΔH_{LDA} values of all additional structures forced upon us by the predictions of subsequent iterations of the outer loop of Fig. 3. Table II also lists the predicted ΔH_{CE} values that caused the structure to be included into the input set and ΔH_{CE} given by the "final" CE selected in the last outer-loop iteration. These data are also presented graphically in Fig. 5, with the inputs of different iterations shown in different colors.

TABLE II. LDA formation enthalpies ΔH_{LDA} (in meV) of $Au_{1-x}Pd_x$ compounds added to the set of the input structures over the iterations of the outer CE loop. Also shown are the range of predicted ΔH_{CE} at the step that caused the structure to be included into the input set and the fitted ΔH_{CE} of the final CE.

x	Structure	Description	Predicted ΔH_{CE}	ΔH_{LDA}	Final ΔH_{CE}
		Step 2			
1/9	A_8B	(301) A_8B SL	−45.1···−38.5	−39.4	−38.6
1/6	A_5B	(301) A_5B SL	−59.5···−55.9	−57.4	−57.3
1/5	A_4B	(201) or (301) A_4B SL	−71.3···−67.9	−67.3	−67.3
5/12	A_7B_5	(302) $A_2B_2A_3B_2A_2B$ SL	−91.3···−89.1	−93.7	−93.7
		Step 3			
1/5	$A_{12}B_3$	(301) A_5BABA_6B SL	−71.0···−67.9	−67.5	−68.5
4/15	$A_{11}B_4$	(401) A_5BABA_4BAB SL (2D LPS, see Fig. 14)	−86.6···−84.9	−85.4	−85.7
2/5	A_9B_6	(401) $A_4B_4A_4BAB$ SL	−92.9···−91.6	−93.6	−89.5
2/3	A_4B_8	(302) $B_5A_2B_3A_2$ SL	−69.0···−63.2	−58.7	−62.4
	A_2B_4	(301) A_2B_4 SL	−68.6···−66.4	−59.1	−58.4
		Step 4			
2/11	A_9B_2	(301) A_5BA_4B SL	−64.9···−62.3	−62.5	−63.9
1/3	$A_{10}B_5$	(401) $A_4BABA_2BA_2BAB$ SL	−91.9···−87.8	−87.8	−87.9
	A_8B_4 (No. 4905)	(302) $A_5B_2A_3B_2$ SL	−95.7···−85.4	−91.1	−88.2
2/5	A_3B_2	(110) A_2BAB SL	−94.0···−86.7	−89.4	−89.8
5/8	A_3B_5	(401) B_4A_2BA SL	−75.6···−68.2	−64.1	−66.6
2/3	A_4B_8	(601) B_6ABA_2BA SL	−68.2···−61.6	−60.7	−59.7
		Step 5			
1/6	$A_{10}B_2$	(not a SL)	−62.2···−54.2	−55.3	−55.3
1/5	A_8B_2	(not a SL)	−71.5···−66.5	−66.5	−67.4
1/3	A_8B_4 (No. 4557)	$A_3BA_2BA_3B_2$ (201) SL	−91.2···−88.8	−91.1	−90.4
7/12	A_5B_7	(302) $B_2A_2B_3A_2B_2A$ SL	−94.4···−91.9	−74.8	−77.2
		Step 6			
1/9	$A_{18}B_2$	(not a SL)	−37.9···−34.8	−34.4	−35.0
2/17	$A_{15}B_2$	(401) $A_{14}BAB$ SL	−43.0···−41.4	−41.0	−41.3
4/17	$A_{13}B_4$	(401) A_6BABA_5BAB (2D LPS, see Fig. 14)	−81.5···−78.9	−79.9	−80.4
1/2	A_3B_3 (No. 55)	(111) A_3B_3 SL	−41.3···−7.4	−11.6	−11.7
		Step 7			
1/11	$A_{10}B$	(301) $A_{10}B_1$ SL	−32.7···−31.7	−31.4	−32.2
2/13	$A_{11}B_2$	(301) A_6BA_5B SL	−54.7···−53.2	−53.3	−54.6

IV. TYPE AND RANGE OF INTERACTIONS REQUIRED FOR DESCRIBING LPS

For the Au-Pd system, an accurate description of the family of $L1_2$-based LPS's is very desirable, since we predict that the ground states of both Au_3Pd ($D0_{23}$) and $AuPd_3$ ($L1_2$) belong to this family. In Table III, we present $\bar{\Pi}_f(\sigma)$ ($\sigma=L1_2$, $D0_{22}$, $D0_{23}$) for the first 12 pairs and for the 2 smallest three-body and the smallest four-body MBIT's. This table demonstrates two general relationships (also obeyed by the MBIT's beyond those included in the table):

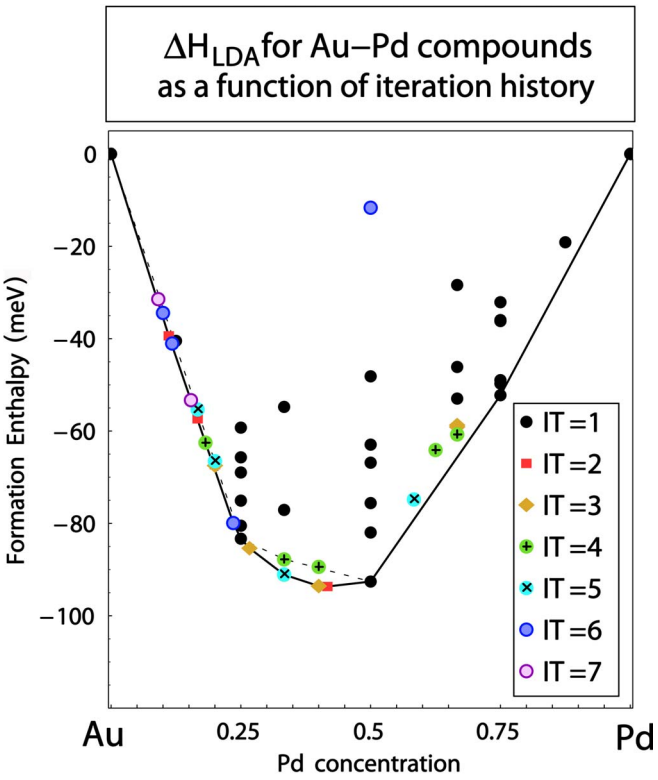

FIG. 5. (Color online) The LDA input set for all iterations $i \equiv \mathrm{IT}$. The original inputs and corresponding convex hull of the first outer-loop iteration IT=1 are represented by the black dots and dashed line; the LDA inputs added at later iterations are represented by colored dots. The solid line shows the final LDA convex hull.

(a) The pair and generally even-body MBIT's have identical $\bar{\Pi}$'s for the structures obtained by the interchange of A and B species (e.g., for A_3B and AB_3 $L1_2$). Thus, three- and generally odd-body MBIT's are needed to obtain an energetic order that is different for A_3B and AB_3 compounds.

(b) For all the MBIT's limited to the first seven nearest-neighbor shells, $\bar{\Pi}$'s for $L1_2$, $D0_{22}$, and $D0_{23}$ are related by

$$\bar{\Pi}_f(D0_{23}) = [\bar{\Pi}_f(L1_2) + \bar{\Pi}_f(D0_{22})]/2. \quad (11)$$

To understand the consequences of (a) and (b), consider the following four "levels" of cluster expansions, depending on the type of MBIT's used. Our point is that reproducing the LPS energetics of Au-Pd requires the highest (No. 4) level of theory.

Level 1. CE's that use only pair interactions (plus the usual J_0 and J_1 terms) and do *not* use pairs beyond the seventh nearest-neighbor shell. In those CE's, the energy of $\Delta H(D0_{23})$ will be exactly the average of $\Delta H(D0_{22})$ and $\Delta H(L1_2)$. Therefore, only two hierarchies of energies are possible, either $L1_2 < D0_{23} < D0_{22}$ or $D0_{22} < D0_{23} < L1_2$, and the separation between the three energies will be identical for A_3B and AB_3 compounds. This conflicts with the LDA [Fig. 2(a)].

Level 2. CE's that use only pair interactions but include pairs of arbitrary length. Including larger pairs allows one to reproduce any conceivable order of $L1_2$, $D0_{22}$, and $D0_{23}$. However, this order and the separation between the three structures will be same for A_3B and AB_3 compounds. This conflicts with the LDA [Fig. 2(a)].

Level 3. Now let us add many-body MBIT's, but only those restricted to the seventh nearest-neighbor shell. This changes the difference $\Delta H(D0_{22}) - \Delta H(L1_2)$ independently in A_3B and AB_3 compounds. However, the large pair interactions of level 2 will remain the only terms contributing to the differences between $\Delta H(D0_{23})$ and the average $[\Delta H(D0_{22}) + \Delta H(L1_2)]/2$, the quantity visualized as δ in Fig. 2. Therefore, $\delta(A_3B)$ and $\delta(AB_3)$ must be identical. It follows that a level-3 cluster expansion has enough degrees of freedom to correctly reproduce the *ground states* at both A_3B and AB_3 compositions; however, it can not always correctly reproduce the *hierarchy* of the $L1_2$-based superstructures. For example, if at AB_3 composition $D0_{23}$ is a ground state, then at A_3B composition $D0_{23}$ cannot be above *both* $L1_2$ and $D0_{22}$, since $\delta = \Delta H(D0_{23}) - [\Delta H(D0_{22}) + \Delta H(L1_2)]/2$ needs to be negative. On the contrary, LDA data for Au-Pd [Fig. 2(a)] show that $D0_{23}$ is the lowest-energy structure at $AuPd_3$, yet at Au_3Pd composition $D0_{23}$ is above both $L1_2$ and $D0_{22}$.

Level 4. Finally, CE's that utilize both pair and many-body MBIT's including at least the eighth nearest-neighbor shell can simultaneously reproduce an arbitrary energetic order of $L1_2$, $D0_{22}$, and $D0_{23}$ in both A- and B-rich compounds. This agrees with the LDA.

TABLE III. Structure-averaged spin products $\bar{\Pi}_f(\sigma)$ given by Eq. (4) of the $L1_2$, $D0_{22}$, and $D0_{23}$ structures for the first 12 pairs and the 3 smallest many-body MBIT's. The interatomic separation vectors in pairs 9 and 10 (with identical distance) are (3,3,0) and (4,1,1), correspondingly. $\bar{\Pi}_f$'s that conflict the sum rule of Eq. (11) are highlighted in bold.

	$\bar{\Pi}$(pairs)												$\bar{\Pi}$(triangles)		$\bar{\Pi}$(tetrahedra)
Compound	1	2	3	4	5	6	7	8	9	10	11	12	First NN	Second NN	First NN
$L1_2$ A_3B	0	1	0	1	0	1	0	**1**	0	**0**	**1**	0	1/2	−1/2	−1
$D0_{22}$ A_3B	0	2/3	1/3	1/3	0	0	1/3	**1**	0	**0**	**2/3**	1/3	1/2	−1/6	−1
$D0_{23}$ A_3B	0	5/6	1/6	2/3	0	1/2	1/6	**2/3**	0	**1/3**	**1/2**	1/6	1/2	−1/3	−1
$L1_2$ AB_3	0	1	0	1	0	1	0	**1**	0	**0**	**1**	0	−1/2	1/2	−1
$D0_{22}$ AB_3	0	2/3	1/3	1/3	0	0	1/3	**1**	0	**0**	**2/3**	1/3	−1/2	1/6	−1
$D0_{23}$ AB_3	0	5/6	1/6	2/3	0	1/2	1/6	**2/3**	0	**1/3**	**1/2**	1/6	−1/2	1/3	−1

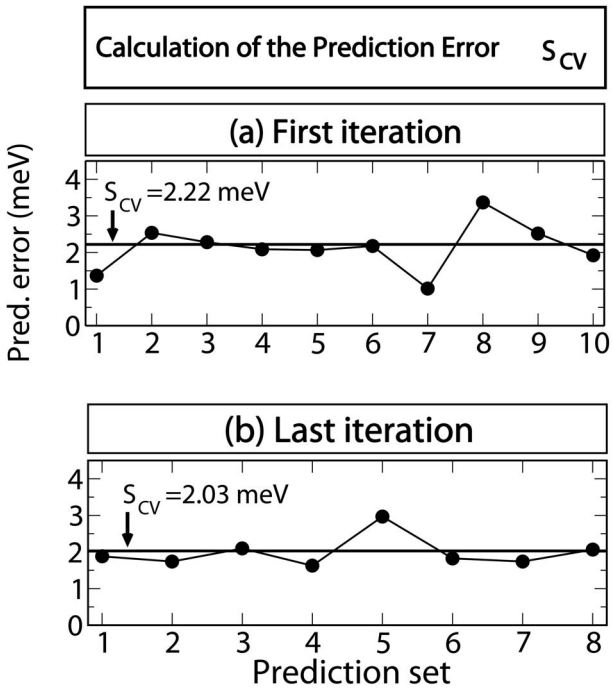

FIG. 6. Calculation of the cross-validation prediction score $S^i_{CV}(\nu)$. Panel (a) shows the best CE candidate ν in iteration $i=1$; panel (b) shows the final CE ($i=7$). In each case, the prediction score S_{CV} (horizontal line) is the average of the prediction errors (dots) for $b^{(i)}$ distinct subdivisions into fitting and prediction sets [Eq. (6)].

It is clear that a level-4 theory is needed for Au-Pd, whereas, say, for Cu-Pd a level-3 theory suffices[81] [cf. the energetic order for Cu-Pd, Fig. 2(b)]. In fact, a level-3 cluster expansion has been successfully established for the Cu-Pd system.[82]

Recognizing that an accurate description of LPS's is a major goal of our study, we observe the following complication: Since all the input structures contribute equally to CV given by Eq. (6), a level-3 CE may have a relatively low CV score even if it makes large errors for the few important LPS's, but gives an excellent description of the many (less important) other input structures. We will mandate a level-4 theory in the following way: (i) we will select MBIT's (by means of a genetic algorithm; see Sec. II) from a pool corresponding to level-4; (ii) we will exclude those MBIT combinations suggested by the GA that lead to only level-3 CE; (iii) we will guide the GA to favor level-4 by assigning larger fit weights to $L1_2$, $D0_{22}$, and $D0_{23}$, but *only* during the trial fits performed by the GA for estimating CV of different CE's. Once the CE's with low CV score have been identified by the GA and the level-3 candidates have been excluded according to (ii), we will refit the numerical values of the pair and many-body interactions, this time assigning same weights to LPS's as to all other structures. In this way we ensure that each resulting CE is *capable* of reproducing the LPS hierarchy, yet is not *forced* to do so by the fit weights.

To illustrate the distinction between the capabilities of a level-3 and a level-4 theory in describing the LPS energetics of Au-Pd, we will apply the procedures described in the previous paragraph beginning with the *second* iteration of the outer loop of Fig. 3. In contrast, we will limit the cluster expansions in the *first* iteration to level 3 by properly restricting pool of MBIT's available to the GA.[83] We will see that for Au-Pd, a level-3 cluster expansion fails not only to fit the $L1_2/D0_{22}/D0_{23}$ energetic order, but even to reproduce the correct ground state; it then further fails to predict the existence of other $L1_2$-based ground states that are identified using a level-4 cluster expansion.

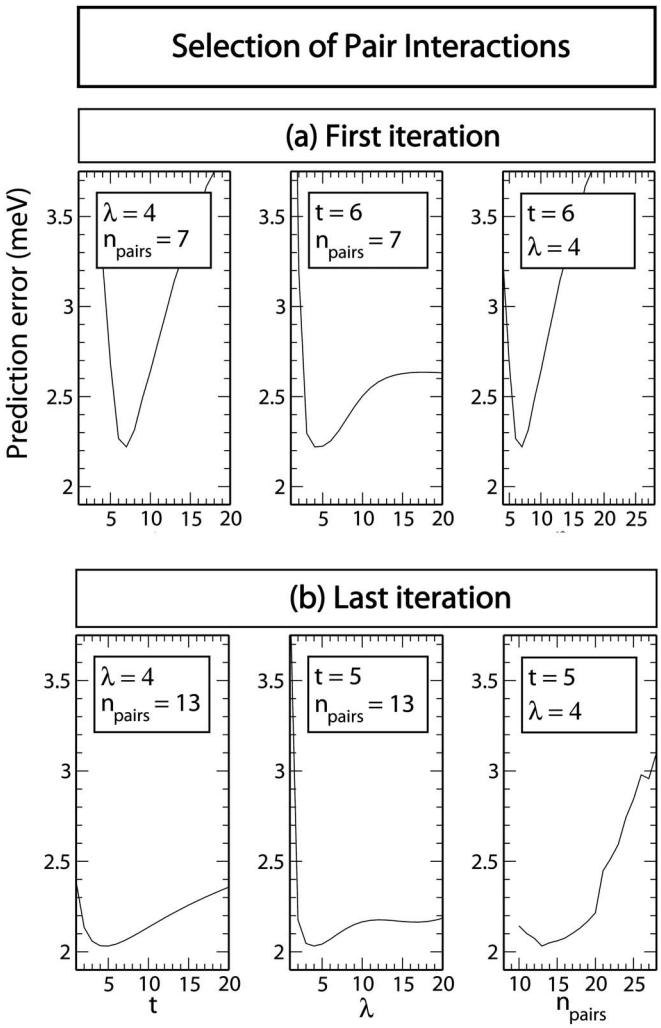

FIG. 7. Selection of pair interactions by minimizing the prediction score S_{CV} for (a) best CE candidate in outer-loop iteration $i=1$ and (b) final CE (outer-loop iteration $i=7$).

V. CONVERGENCE OF THE CLUSTER EXPANSION

A. Inner loop: Identification of MBIT's for Au-Pd

The selection of pair interactions and MBIT's in the inner loop is governed by the leave-many-out cross-validation score $S^i_{CV}(\mathrm{CE}_\nu)$ [Eq. (6)] for a candidate CE_ν in iteration i. We illustrate the calculation of the CV score in Fig. 6. Part (a) shows the results for the best CE found in the first iteration $i=1$ of the outer loop and (b) the results for the final CE selected in the last iteration $i=7$ of the outer loop. The numbers $b^{(i)}$ of distinct subdivisions into fitting sets and predic-

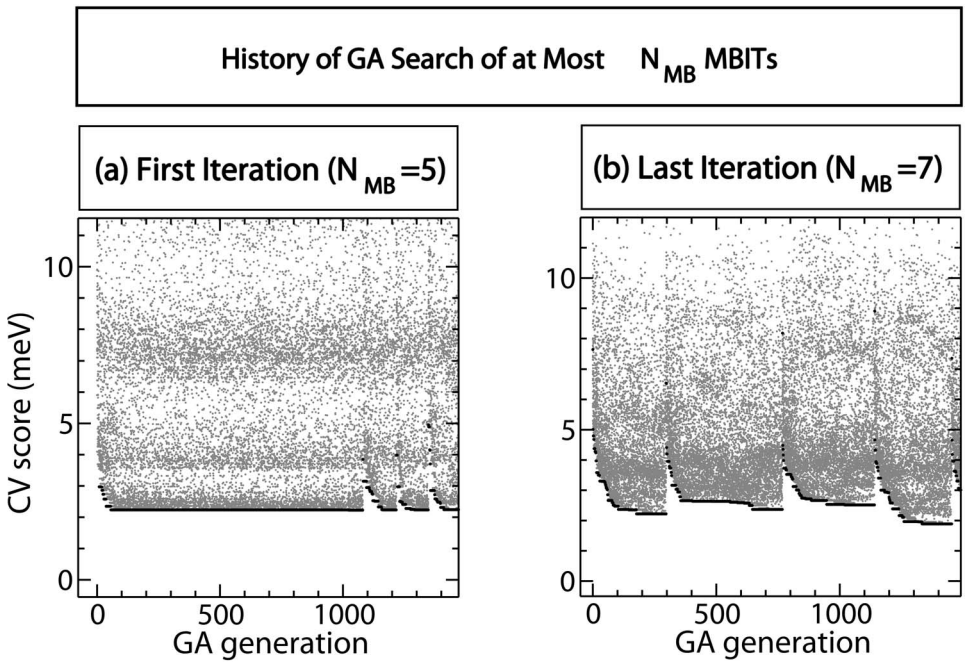

FIG. 8. Genetic algorithm (GA) search of the optimal many-body interaction types (MBIT's). The search is repeated for different values of maximum number N_{MB} of MBIT's; shown are examples for (a) $N_{MB}=5$ in iteration $i=1$ of the outer loop and (b) $N_{MB}=7$ in iteration $i=7$. In each generation, there are a number of trial cluster expansions (CE's) with different CV prediction scores (gray dots). As new trial CE's are produced via mating and mutations, the CEs with high CV score "die out." The black dots denote the best CE at each generation; when its prediction score stops improving, the best CE is "locked out" and a new population is generated [e.g., at generations 1080, 1217, and 1347 in panel (a)]. For visual clarity, only first 1500 GA generations are shown, although the GA is run until the new "locked-out" individuals appear with consistently higher CV score than those already known (typically ~5000 generations).

tion sets are $b^{(1)}=10$ and $b^{(7)}=8$. We see that the prediction error constitutes no more than a few meV for the various subdivisions of the input set into fit and prediction subsets.

We illustrate the selection of pair interactions via the $t-\lambda$ criterion [Eq. (8)] in Fig. 7.[84] The constrained fit of Eq. (8) allows one to use a large number of pairs without overfitting; the first two plots in Fig. 7 illustrate how the predictive power of the resulting cluster expansion depends on the parameters that define those constraints. From the last plot in Fig. 7 we see that in the first outer-loop iteration ($i=1$) S_{CV} is minimized when only $n_{\text{pairs}}=7$ pairs are used ($t=6$ and $\lambda=4$), while $n_{\text{pairs}}=13$ pairs are needed in the last outer-loop iteration ($i=7$).

We illustrate the selection of MBIT's in Figs. 8 and 9. In Fig. 8 we show how the GA search proceeds for $N_{MB}=5$ MBIT's in iteration $i=1$ and for $N_{MB}=7$ MBIT's in iteration $i=7$ (at each iteration i, we vary the allowed number N_{MB} of nonzero interactions and perform a separate GA run for each N_{MB}). In general (since the amount of input data is limited) there will be not one but several possible "families" of MBIT's which yield a low S_{CV}—i.e., sets of good candidate cluster expansions differing by very few MBIT's within a given set but by several MBIT's from the cluster expansions in different "families." Such families correspond to local minima in the GA search space. To find a different family, we employ a "lock-out" mechanism;[62] i.e., the GA is periodically restarted after a low-S_{CV} solution persists for too long and said low-S_{CV} is forbidden to recur ever again in the remaining run. We see that already in the first outer-loop iteration ($i=1$) the GA search finds a substantial number of cluster expansions with low CV score ($S_{CV}<2.5$ meV). In fact, in $i=1$ there are so many candidate cluster expansions with low CV score that it takes more than 1000 iterations to lock out the first local optimum. This indicates that the restricted LDA input set can be equally well described by different cluster expansions in iteration $i=1$. Many of those early cluster expansions lead to incorrect predictions for new structures, but as those structures are added to the input set, the CV score increases for those "incorrect" cluster expansions, but not for those cluster expansions that in fact give correct predictions. Accordingly, in the last iteration $i=7$ the GA rapidly finds the best cluster expansion in each of the families differing by only few MBIT's. We see that in $i=7$ different families have quite different CV scores, and the best family is found only on the fourth attempt (in GA generation 1453). The GA is run until the new locked-out individuals appear with consistently higher CV score than those already known (typically ~5000 generations).

Figure 9 illustrates the selection of "optimal" N_{MB}—i.e., the number at which $S_{CV}(N_{MB})$ levels out, thus providing good predictions yet avoiding overoptimization. The CV score first decreases as we increase the number N_{MB} of MBIT's, and then flattens out at what we identify as the "optimal" value N_{MB}^{opt}. For the first iteration one can identify $N_{MB}^{opt}=5$, while in the last iteration $N_{MB}^{opt}=7$. While occasional CE candidates with $N_{MB}>N_{MB}^{opt}$ have slightly lower CV scores, they do not present substantial improvement, but carry a higher risk of CV overoptimization. We thus consider only CE candidates with $N\leqslant N_{MB}^{opt}$.

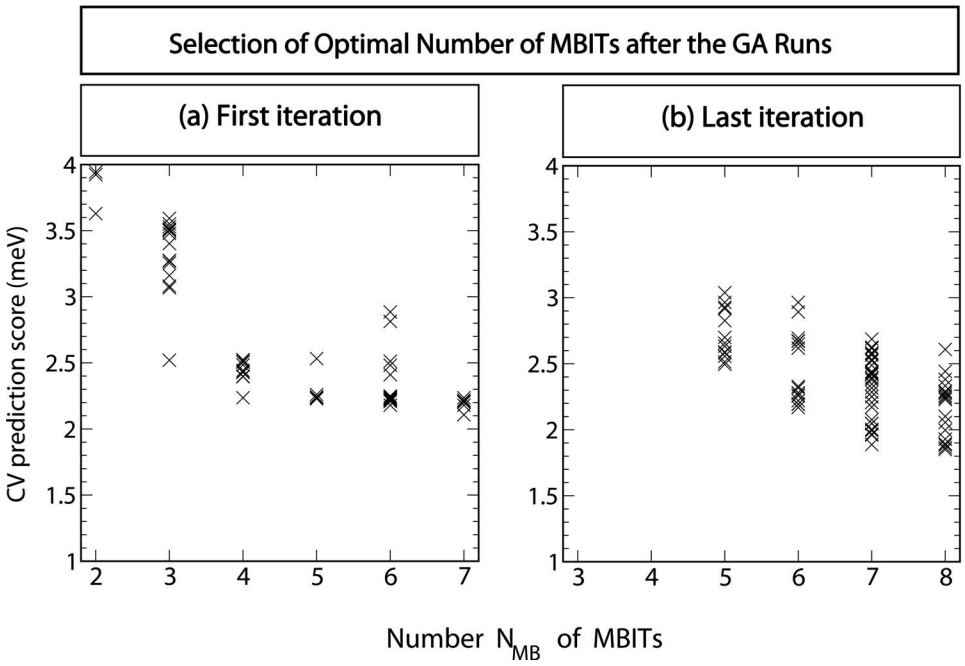

FIG. 9. The prediction errors of the CE candidates found by the GA (a) in the first outer-loop iteration $i=1$ and (b) in the last iteration $i=7$ of the outer loop vs the maximum number N_{MB} of many-body interaction types (MBIT's) that the GA was allowed to use.

B. Outer loop: Selection of structures for constructing the CE

1. Ground-state search at different outer-loop iterations

In Fig. 10 we illustrate the ground-state searches carried out for the best CE candidates of the first and last iterations of the outer loop ($i=1$ and $i=7$). The dots denote the energies of all possible structures with up to 16 ($i=1$) or up to 20 ($i=7$) atoms per unit cell, while the lines indicate the convex hull that bounds those energies from below. The breaking points of this convex hull are indicated by arrows; as we saw in Fig. 4, each such a breaking point is a predicted ground state.

We repeat the ground-state search for the other selected CE candidates (cf. Fig. 9). For iteration $i=1$, the predictions of all the selected CE candidates are summarized in Table IV. Since different CE candidates may predict different ground states, we list the fraction of the selected CE's which support a particular ground-state prediction. Nine structures

TABLE IV. First iteration: the ground-state predictions of the ten CE's analyzed in the first iteration of the outer loop, compared to the LDA data. For each structure σ we indicate how many CE candidates predict that σ is a ground state, the lowest predicted depth $\Delta(\sigma)$ [see Eq. (10)], and the range of $\Delta H_{CE}(\sigma)$ given by different CE candidates. Ground-state predictions satisfying our criteria (i)–(iv) of Sec. II D are highlighted in bold. In the last two columns, "n/a" means that no LDA calculations were performed for the indicated structure, while "∼" indicates that the structure has $\Delta(\sigma)=0$ in the LDA. Note that while all the CE candidates have a low CV score, their ground-state predictions are not very consistent, indicating that further iterations of the outer CE loop (cf. Fig. 3) are needed.

	Structure		CE predictions			LDA data	
x	Name	Description	How often	Lowest depth (meV)	ΔH_{CE} range (meV)	ΔH_{LDA} (meV)	Convex hull breaking point?
0.1111	$\boldsymbol{A_8B}$	(301) A_8B SL	**100%**	**5.5**	−45.1···−38.5	−39.4	∼
0.1250	$A_{14}B_2$	(301) A_6BA_8B SL	40%	0.1	−49.1···−43.1	n/a	n/a
0.1667	$\boldsymbol{A_5B}$	(301) A_5B SL	**30%**	**1.9**	−59.5···−55.9	−57.4	No
0.2000	$\boldsymbol{A_4B}$	(301) A_4B SL	**80%**	**2.3**	−71.3···−67.9	−67.3	No
0.2500	$\boldsymbol{D0_{22}}$	(201) A_3B SL	**100%**	**8.7**	−83.5···−81.9	−80.5	No
0.3333	$\boldsymbol{\gamma 1}$	(201) A_2B SL	**90%**	**3.0**	−89.0···−87.9	−87.8	Yes
0.3750	$A_{10}B_6$	$A_2B_2A_3BA_3B_2A_2B$ (203) SL	30%	0.9	−90.5···−89.2	n/a	n/a
	$A_{10}B_6$	Not a SL	50%	0.9	−90.6···−89.3	n/a	n/a
0.4167	$\boldsymbol{A_7B_5}$	See Fig. 14	**80%**	**1.5**	−91.3···−89.1	−93.7	Yes
0.4286	A_4B_3	(201) $A_2B_2A_2B$ SL	20%	0.6	−91.2···−89.7	n/a	n/a
0.5000	**CH**	(201) $\boldsymbol{A_2B_2}$ SL	**100%**	**14.4**	−91.8···−89.1	−92.6	Yes
0.7500	$\boldsymbol{L1_2}$	AB_3, not a SL	**40%**	**6.3**	−51.1···−50.0	−52.2	Yes
	$\boldsymbol{D0_{22}}$	(201) AB_3 SL	**60%**	**5.3**	−51.2···−48.4	−49.7	No

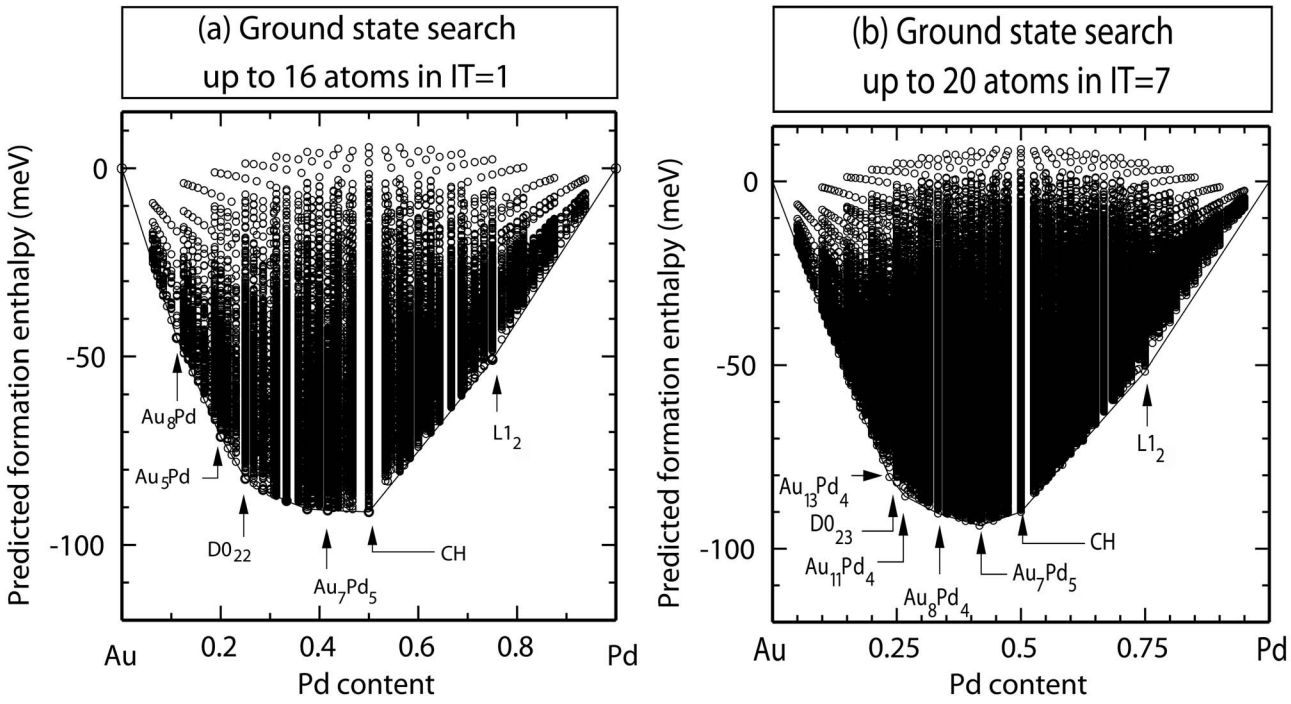

FIG. 10. Results of a direct-enumeration ground-state search for the cluster expansion candidate with the lowest CV score in outer-loop iterations (a) $i=1$ and (b) $i=7$ (final CE). Arrows point to the major ground states.

satisfy our "importance" criteria set forth in Sec. II (predictions that are either "deep" or "frequent"); those structures are highlighted in bold and will be considered the predictions of iteration $i=1$.

2. Illustrating the outer-loop history

We illustrate pictorially the outer-loop history and the agreement (or disagreement) between the CE predictions and the LDA energies for all outer-loop iterations in Fig. 11. In that figure, each structure is represented by a square, with its upper triangle representing the CE predictions and the lower triangle the actual LDA data. If the structure is a ground-state prediction in CE (or a breaking point in the LDA), the corresponding triangle is black; if the structure is *not* a ground-state prediction (or a breaking point), the corresponding triangle is white. In cases when the LDA and CE results are too close to call but formally disagree, the squares are shaded as reflected in the figure's legend. For visual clarity, we do not distinguish the competing $L1_2$-based structures ($L1_2/D0_{22}/D0_{23}$) in Fig. 11, but illustrate the CE success in describing those structures in Table V.

It is interesting to observe how the selection of input structures in outer-loop iterations produces different CE's and how the outer loop converges to a remarkably accurate CE. The first column under the IT=1 heading in Fig. 11 compares the predictions of the first outer-loop iteration $i=1$ (cf. Table IV) to the breaking points on the convex hull of the LDA input of $i=1$. We see the following.

(i) *CE predictions in agreement with LDA input*. Two predicted ground-state structures $Au_2Pd\gamma 1$ and Au_2Pd_2 CH were already LDA breaking points.

(ii) *CE predictions in conflict with LDA input*. Besides the $L1_2$-based structures whose subtle hierarchy was not reproduced correctly in IT=1 (cf. Table V), all LDA breaking points were predicted as ground states.

(iii) *New ground-state predictions*. The CE predicts four new ground states that were not in the input. These are Au_8Pd $[(301)A_8BSL]$, Au_5Pd $[(301)A_5BSL]$, Au_4Pd $[(301)A_4BSL]$, and Au_7Pd_5.

The second column under the IT=1 heading in Fig. 11 describes the result of the LDA test for the new predictions.

TABLE V. Percent of CE candidates correctly reproducing the lowest $L1_2$-based long-period superstructure and the correct hierarchy of $L1_2$-based structures, at compositions Au_3Pd and $AuPd_3$, for different iterations of the outer loop.

Composition	Percent of CE candidates reproducing:	$N=28$ IT=1	$N=32$ IT=2	$N=37$ IT=3	$N=43$ IT=4	$N=47$ IT=5	$N=51$ IT=6	$N=53$ IT=7
Au_3Pd	LDA-confirmed lowest-energy structure ($D0_{23}$)	0%	88%	92%	62%	64%	100%	100%
Au_3Pd	LDA $L1_2/D0_{22}/D0_{23}$ hierarchy	0%	88%	92%	62%	64%	100%	100%
$AuPd_3$	LDA-confirmed lowest energy structure ($L1_2$)	40%	100%	100%	92%	79%	100%	100%
$AuPd_3$	LDA $L1_2/D0_{22}/D0_{23}$ hierarchy	0%	37%	100%	85%	79%	100%	100%

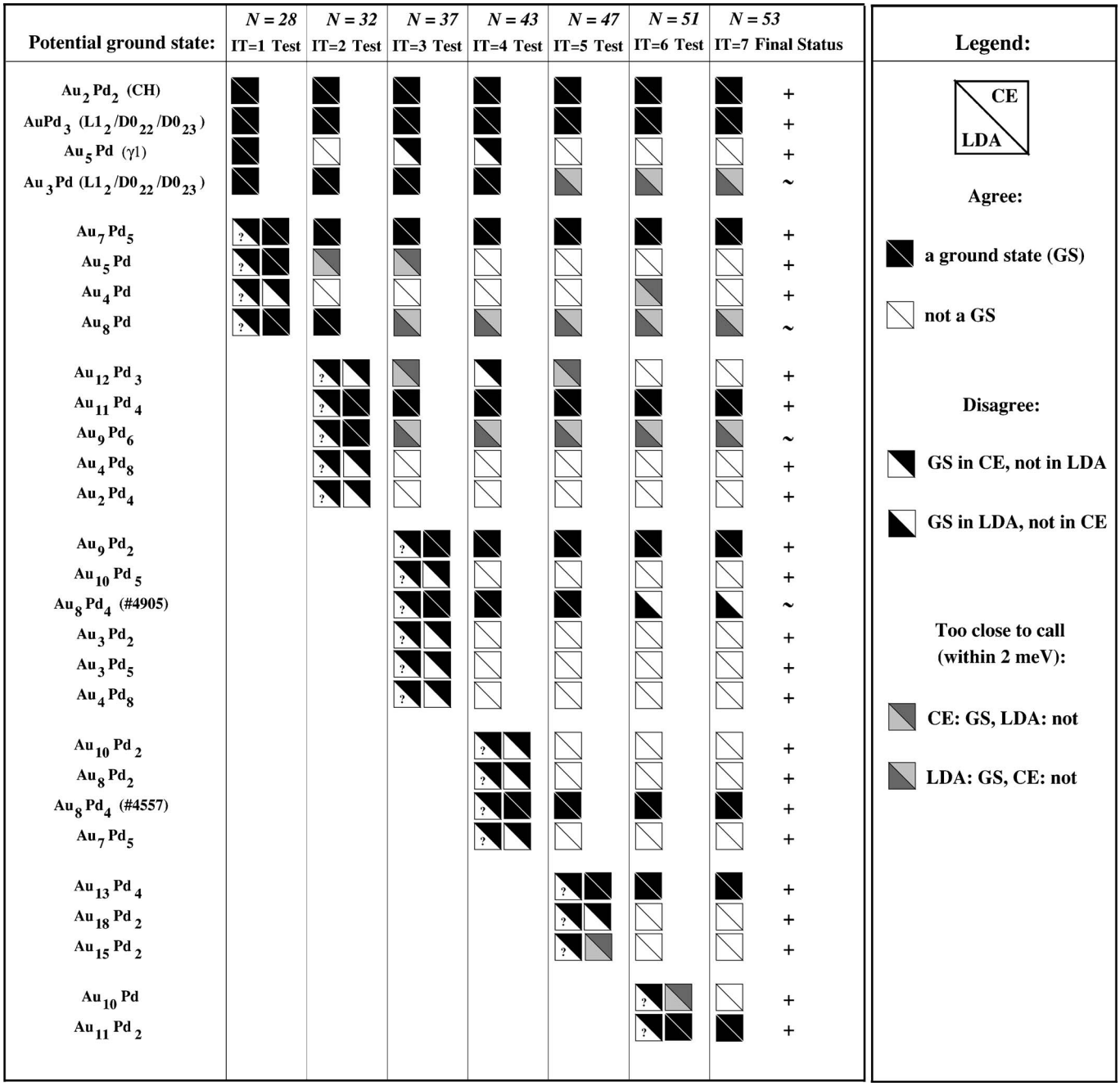

FIG. 11. Evolution of the ground-state predictions over the outer-loop iterations. Each structure is represented by a square, with the upper part representing the CE predictions and the lower part representing the actual LDA data, as summarized in the legend.

We see the following.

(i) *CE predictions in agreement with the LDA test*. The LDA confirms the CE predictions for Au_8Pd, Au_5Pd, and Au_7Pd_5.

(ii) *CE predictions in conflict with the LDA test*. The LDA disagrees with the CE prediction of Au_4Pd which is not confirmed to be a new ground state.

(iii) *Structures removed from the LDA convex hull*.[85] When we calculated ΔH_{LDA} for the structure Au_7Pd_5, we found that it was so low that it removes the structure Au_2Pd ($\gamma 1$) from the LDA convex hull.

3. Generic behaviors during outer-loop iterations

Looking at the results of *all* of the outer-loop iteration history summarized in Fig. 11, we see that there are a number of possible generic evolution scenarios for a particular structure over the outer-loop iteration history, as follows.

(a) A correct ground-state structure can be included into the initial input set by chance (and thus be successfully predicted throughout all the iterations), as happened, e.g., with CH and $AuPd_3$ $L1_2$.

(b) A structure that was a prominent breaking point of the original LDA convex hull, and even one that was predicted

to be a deep ground state in the *first* outer-loop iteration, may finally turn out *not* to be a ground state, as happens with $\gamma 1$.

(c) Before the outer-loop iterations have converged, the CE and LDA can reach an apparent agreement at some point ($i=2$ for $\gamma 1$) and then disagree for a few iterations ($i=3,4$) before finally reaching consensus.

(d) A correct ground state may be first identified both early (Au_7Pd_5) and late ($Au_{11}Pd_2$) in the outer-loop iteration history.

From Fig. 11 we see that most of the ground states (black squares in the IT=7 column) did not enter the *initial* input set. This signifies the importance of an exhaustive ground-state search, able to identify the ground-state structures that would be otherwise unsuspected. On the other hand, a single CE fit followed by an exhaustive ground-state search is insufficient, as is evident from the many mistakes CE made in early outer-loop iterations. Thus, several outer-loop iterations are required to ensure the accuracy of the CE predictions.

To better understand how the CE predictions change during the outer-loop iterations, consider Fig. 5. In that figure, black dots denote ΔH_{LDA} for the structures used in the initial LDA input set, while color dots denote ΔH_{LDA} for those structures added during the iterations of the outer loop. First, consider the Pd concentration range $1/2<x<3/4$. We see that ΔH_{LDA} for all the color dots in this range lie substantially above the convex hull ($\Delta \sim 5$ meV). However, each of those structures was predicted to be a deep ($\Delta \sim -5$ meV) ground state in one of the early iterations of the CE. Thus, the initial LDA input set did not have sufficient data for the CE to accurately describe this concentration range and needed to be supplemented before the CE could make the *qualitatively* correct predictions. Second, *in the range* $1/4<x<1/2$, the data in the initial LDA set were sufficient to predict the prominent ground-state Au_5Pd_7 as early as in the first iteration. Yet reproducing the details of the ground-state line required additional input at later iterations, as evidenced by the many ground-state predictions (color dots) lying well above the convex hull in this region. Finally, *in the range* $0<x<1/4$, all the added ΔH_{LDA} lie on, or close to, the final convex hull (and were predicted with an accuracy of a few meV—cf. Table II). Thus, the initial LDA input already allowed quite an accurate quantitative description of this range.[86] We thus learn that the role of the outer loop may be different for different physical regions (such as different x ranges). Even if CE appears very successful in describing some region at the very first outer-loop iteration, complete outer-loop convergence is essential to ensure the reliability of the CE predictions.

4. Testing high-energy predictions

Before concluding that our CE has fully converged, we also compared $\Delta H_{CE}(\sigma)$ predicted by different CE candidates for *all* ~3 000 000 structures σ up to 20 atoms per cell (not just ground states). When we first made this comparison in $i=5$, we found that $\Delta H_{CE}(\sigma)$ values predicted by different CE candidates for the same structure σ were *usually* but *not always* close: in the worst case of Au_3Pd_3 ("No. 55"), it predicted that ΔH_{CE} (No. 55) differed by over 30 meV (cf. Table II). This was because the ΔH_{LDA} values added to inputs before $i=5$ were intended to improve the cross-validation and CE predictions for the low-energy structures (those near the ground-state line), but not necessarily for all high-energy structures. In subsequent iterations $i=6$ and $i=7$, after having added ΔH_{LDA} (No. 55) to the inputs, the predictions of different CE candidates became *always* consistent, differing by $\leqslant 4.2$ meV for all structures. This indicates that the outer loop has converged with respect to the high-energy as well as the low-energy structures.

From $i=7$ column of Fig. 11, we see that out of 28 structures ever predicted as ground states over the outer loop iterations, the LDA and CE agree that 8 structures are indeed ground states (black squares) and the LDA and CE agree that 16 other structures are not ground states (white squares). The final agreement between the CE and LDA is indicated by a "+" sign in the last column of Fig. 11. For three structures Au_3Pd $D0_{23}$, Au_8Pd, and Au_9Pd_6, the LDA and CE disagree about the sign of the depth Δ, but numerically this disagreement is small (less than 2 meV in both cases) as indicated by "~" sign. In addition, over the iterations of the outer loop too *different* Au_8Pd_4 structures (labeled in Fig. 11 as No. 4905 and No. 4557) were suggested as potential ground states, and in fact the two structures turned out to be degenerate in the LDA. It turns out that a single cluster expansion (limited to a reasonable number of terms) has difficulty assigning the same energy to those two structures. In IT=4 and IT=5, both structures are predicted as ground states, however by *different* CE candidates suggested by the GA. As the outer loop converges and the number of good CE candidates is reduced, structure No. 4905 is no longer predicted as a ground state. Yet it is still placed very close to the ground-state line (within 2.2 meV for our final CE), and this acceptable level of error is indicated by a "~" sign in Fig. 11. Overall, there is an excellent agreement between the LDA convex hull and CE predictions (see Table VI).

VI. PREDICTIVE ACCURACY OF THE FINAL CLUSTER EXPANSION

We finally focus on the single best CE found in iteration $i=7$. The MBIT's selected by the GA for that CE are shown in the lower part of Fig. 12(a). In the upper part of Fig. 12(a), we show the numerical values of pair and many-body interactions for that CE. In Fig. 12(b) we show the constituent strain given by Eq. (2). [Remember that the pair and many-body interactions define only $\Delta\tilde{H}_{CE} \equiv \Delta H_{CE} - E_{CS}(\sigma)$, so that the constituent term needs to be added back to obtain ΔH_{CE}]. The left panel of Fig. 12(b) shows the equilibrium energies of infinite-period Au/Pd superlattices of given composition, determined *ab initio* from the elastic properties of pure Au and Pd. Constituent strain for other directions can be obtained by interpolation of those values (at fixed composition) with Kubic harmonics, as illustrated in the right panel of Fig. 12(b). The energetic parameters of Fig. 12 constitute our best available energetic description of Au-Pd, and we select it as the final cluster expansion for our study.

The CV score corresponding to our final CE is 2.4 meV. Frequently, the CV score is regarded as the ultimate measure of the predictive ability.[15,70] However, we saw above that an

TABLE VI. Last iteration: the ground-state predictions of the four CE candidates, compared to the LDA input data. Search up to 20 atoms per unit cell. The data format is same as in Table IV.

	Structure			CE predictions		LDA data	
x	Name	Description	How often	Lowest depth (meV)	ΔH_{CE} range (meV)	ΔH_{LDA} (meV)	Convex hull breaking point?
0.1538	$\boldsymbol{A}_{11}\boldsymbol{B}_2$	(301) A_6BA_5B SL	**100%**	**–0.6**	–54.6···–54.2	–53.3	Yes
0.1818	$\boldsymbol{A}_9\boldsymbol{B}_2$	(301) A_5BA_4B SL	**100%**	**–0.4**	–63.9···–63.6	–62.5	Yes
0.2353	$\boldsymbol{A}_{13}\boldsymbol{B}_4$	LPS, see Fig. 14	**100%**	**–3.2**	–80.8···–80.4	–79.9	Yes
0.2500	$D0_{23}$	LPS, see Fig. 14	0%	0.82	–82.35···–81.97	–83.31	Yes
0.2667	$\boldsymbol{A}_{11}\boldsymbol{B}_4$	LPS, see Fig. 14	**100%**	**–2.1**	–85.9···–85.7	–85.4	Yes
0.3333	$\boldsymbol{A}_8\boldsymbol{B}_4$ (No. 4557)	$A_3BA_2BA_3B_2$ (201) SL	**100%**	**–1.2**	–90.4···–89.9	–91.6	Yes
0.4167	$\boldsymbol{A}_7\boldsymbol{B}_5$	See Fig. 14	**100%**	**–3.5**	–93.7···–93.1	–93.7	Yes
0.5000	**CH**	(201) A_2B_2 SL	**100%**	**–7.6**	–90.7···–90.0	–92.6	Yes
0.7500	$\boldsymbol{L}1_2$	Not a SL	**100%**	**–6.7**	–51.9···–51.0	–52.2	Yes

underconverged CE can make errors by far exceeding its CV score. In fact, S_{CV} only indicates how well CE predicts the energies of the *fixed* set of $\{\Delta H_{LDA}\}$, and the constructed CE is *optimized* to yield a low CV score. Thus, to objectively estimate the predictive power of our final CE, we have calculated 37 *new* $\Delta H_{LDA}(\sigma)$ that were never used during the construction of CE and compared them to the predicted $\Delta H_{CE}(\sigma)$. The results of this comparison are shown in Fig. 13. We see that our final CE can make true predictions with average accuracy of 2.8 meV.

VII. DISCUSSION OF GROUND-STATE ORDERED-STRUCTURES IN $Au_{1-x}Pd_x$

The ground states of AuPd predicted by our final CE (and all confirmed by direct LDA calculation) are shown in Fig. 14. We will discuss the results in four distinct composition ranges.

A. Pd-poor $Au_{1-x}Pd_x$ compounds, $x<0.22$: (301) "adaptive structures"

In Pd-poor concentration range there are no deep ground states; instead, we encounter "adaptive structures,"[87]—i.e., a quasicontinuum of ordered structures sharing a common simple structural motif and all lying on the ground-state line. This shows that the energetics of the system allows for an efficient adaptation to any given alloy composition. Previously, adaptive structures were found for Au-rich Cu-Au and Pt-rich Ni-Pt.[87] Examination of the adaptive structures in Au-Pd shows that they all are formed by (301) planes of pure Pd separated by several (301) planes of pure Au. The region of Au-Pd adaptive structures is indicated by a thick line in Fig. 14. Following Ref. 87, we can analyze this phenomenon in terms of an interplay between the strain energy represented by the "constituent strain" E_{CS} [Eq. (2) and Fig. 12(b)] and the "spin-flip energies"—i.e., the chemical energies obtained by subtracting E_{CS} from ΔH_{LDA}. In the case of $Au_{1-x}Pd_x$, Fig. 12(b) shows that the (001) ordering has the least strain, especially in the Au-rich composition. At the same time, the spin-flip energies are very attractive for the opposite-type nearest-neighbor atoms [as evidenced by the large positive value of the first pair interaction in Fig. 12(a)], making planes with large number of nearest neighbors, such as (001) planes, unfavorable for ordering. Ordering in (301) or (401) leads to lower spin-flip energies while still resulting in small constituent strain. The best compromise is obtained by ordering in (301) planes.

B. Ground-state structures around Au_3Pd composition: Long-period superstructures

Around $x=1/4$, Fig. 14 shows three deep ground-state structures $Au_{13}Pd_4$, $D0_{23}$ (Au_6Pd_2), and $Au_{11}Pd_4$. As discussed in the Introduction and seen in Fig. 1(a), $D0_{23}$ is a well-known one-dimensional long-period superstructure that can be obtained from $L1_2$ structure by introducing (100) antiphase boundaries separated by $M=2$ lattice constants. It turns out that the structures $Au_{13}Pd_4$ and $Au_{11}Pd_4$ also consist of $L1_2$ domains, however separated by *two* orthogonal sets of (401) defect planes, as can be seen in Fig. 14. Thus, $Au_{13}Pd_4$ and $Au_{11}Pd_4$ can be characterized as *two-dimensional* LPS's.[88] Note that in addition to serving as antiphase boundaries, the defect planes in $Au_{13}Pd_4$ and $Au_{11}Pd_4$ introduce the necessary substitutions accounting for the stoichiometric difference with the parent Au_3Pd composition. Thus, we predict that one- or two-dimensional LPS's should be stable at zero temperature at *several* Au-rich compositions.

Regarding the stoichiometric Au_3Pd composition, at which ordering is most commonly anticipated, we note that our predicted ground state $D0_{23}$ (also predicted in Ref. 15) is different from the $L1_2$-ordered state observed at this composition in thin Au-Pd films.[20] Experimentally, $L1_2$ has (001)-type order, while $D0_{23}$ would be characterized by both (401)- and (001)-ordering vectors. We thus conclude that ordering tendencies in *bulk* Au-Pd are different from those reported for thin films.

We finally note that some LPS's observed experimentally in various intermetallic alloys have exceptionally large cells (with more than 20 atoms). This is particularly characteristic of two-dimensional LPS's. Such structures are beyond the

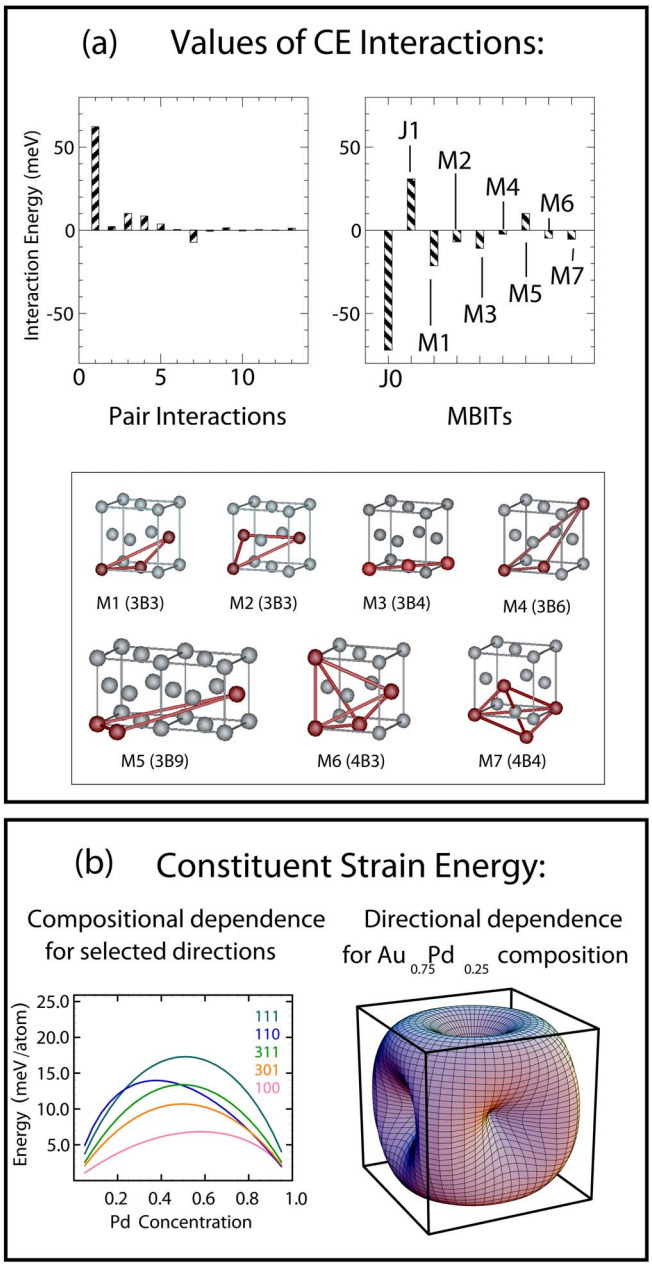

FIG. 12. (Color online) Energetic parameters defining our final cluster expansion (CE): (a) Values of pair interactions (top left) and of the many-body interaction types (MBITs) (top right). The MBITs themselves are shown in the bottom panel of part (a) and were selected by the genetic algorithm in the outer-loop iteration $i=7$. (The MBIT code given in parentheses identifies the number of vertices in a MBIT and the largest separation between those vertices.) (b) Constituent strain energy E_{CS} as given by Eq. (2) in the infinite-period limit, shown for selected directions as a function of composition (left) and for $Au_{0.75}Pd_{0.25}$ composition as a function of superlattice direction. (In the panel showing the compositional dependence of E_{CS}, the top-to-bottom order of labels corresponds to the order of lines at Pd concentrations 0.3–0.4.)

limits of the exhaustive search performed here, which is limited by $N=20$. However, the cluster expansion $E_{CE}(\sigma)$ can be applied to any structure, even one with very large N. It is indeed possible to use the building blocks we have identified

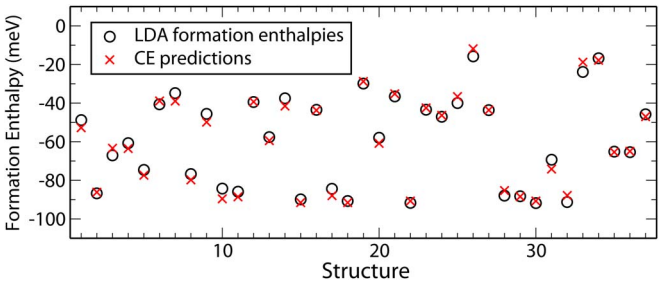

FIG. 13. (Color online) Comparison of the directly calculated ΔH_{LDA} for 37 new structures [never used during construction of CE (circles)] to the corresponding values of ΔH_{CE} predicted by our final CE (crosses). The average prediction error for those completely new structures is only 2.8 meV.

for the LPS's and construct systematically $E_{CE}(\sigma)$ of large, postulated structures, in a search for a possible new type of LPS ground state. Such a study is postponed to a future publication.

C. $Au_{1-x}Pd_x$ compounds at $0.27<x<0.5$: Unsuspected ordered compounds

In the moderately Au-rich concentration range, we find several completely unsuspected ground-state structures. Most striking is the appearance of the structure Au_7Pd_5 (Fig. 14) which has the lowest ΔH_{LDA}. While the experimentally measured formation enthalpy of the *disordered* Au-Pd alloy indeed has the minimum at a similar composition,[17,18] all the earlier theoretical investigations of Au-Pd[15,46,50] have suggested that the *ordered* compound with the lowest ΔH_{LDA} is at the composition $x=1/2$. In fact, as we discussed above, all those earlier theories considered only a limited library of at most $\mathcal{O}(200)$ structures and thus could not account for an fcc ground state at composition $x=5/12$. Our use of a direct enumeration of $\mathcal{O}(10^6)$ structures allows us to identify Au_7Pd_5 as an important structure and to conclude that the ordered and random alloys of the lowest formation enthalpy have similar compositions x.

We further find two distinct Au_8Pd_4 structures that are degenerate in the LDA and thus both should be considered ground states. Several other structures in this composition lay close to the ground-state line. This is similar to the region of adaptive structures at low x, except that for $0.27<x<0.5$ we could not identify any simple structural motif common to the near-ground-state structures.

D. $Au_{1-x}Pd_x$ ground states at $x\geqslant 0.5$

For Pd-rich Au-Pd alloys, we find only two ground states, at compositions $x=1/2$ and $x=3/4$. These are the same compositions at which ordering has been observed in thin Au-Pd films[20,22] and predicted theoretically.[15,46,50] At $x=3/4$, we predict that $L1_2$ structure is stable at $T=0$, as also was suggested by the earlier studies.[46,50] However, contrary to the results of thin film experiments and to some less exhaustive theoretical studies,[46,50] we find that the ground state at $x=1/2$ is a Au_2Pd_2 (201) superlattice structure. This structure

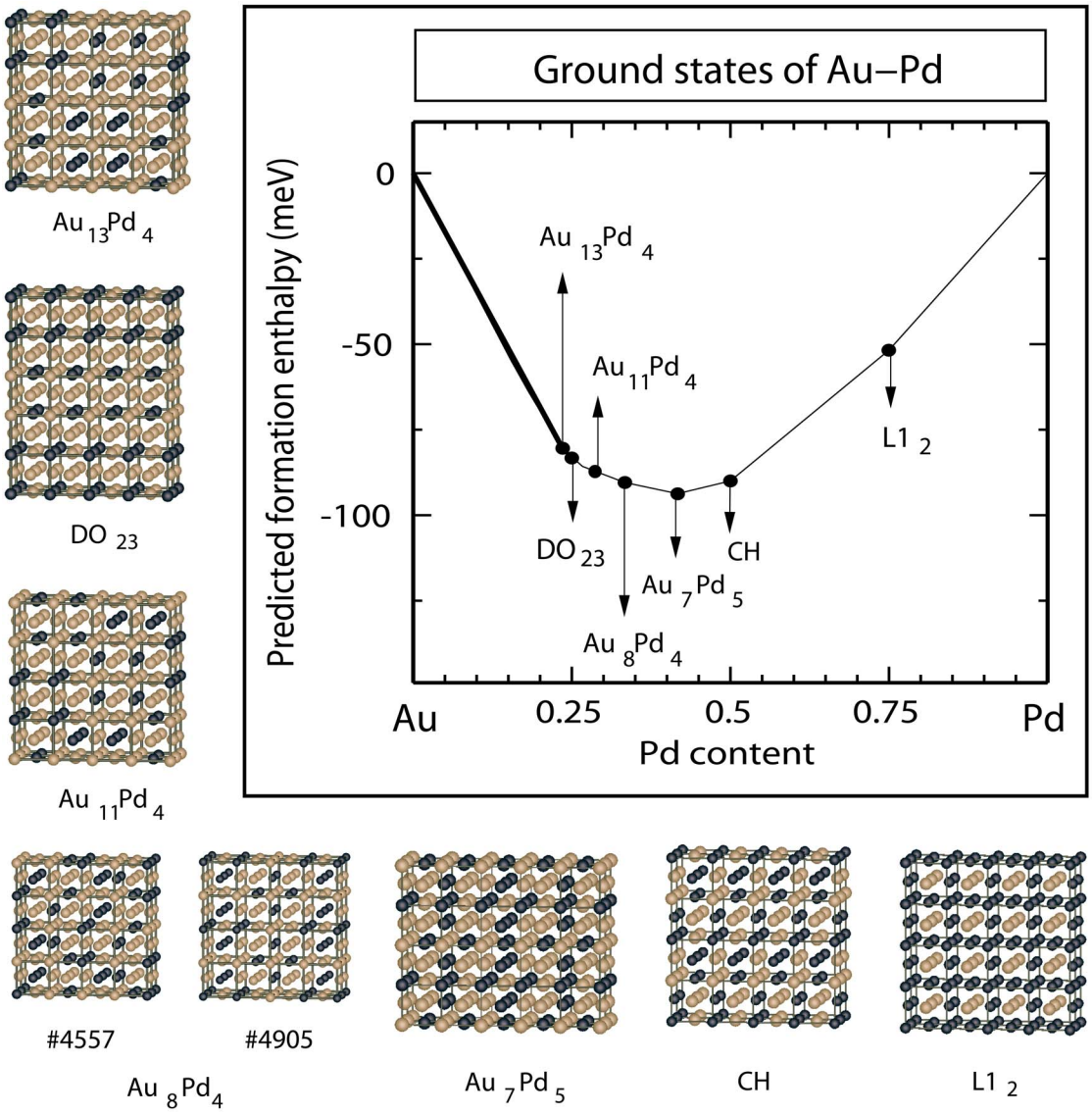

FIG. 14. (Color online) Ground-state structures of the Au-Pd alloy system. The light-golden spheres denote Au atoms, and the dark spheres denote Pd atoms. The thick line at $x<0.22$ signifies a region of "adaptive" structures, in which many ground states and near ground states with negligible depth Δ [given by Eq. (10)] appear. The two Au_8Pd_4 structures (labeled by the number assigned to them by our direct enumeration routine) have the same LDA total energy.

is analogous to the Cu-Fe sublattice of the chalcopyrite ($CuFeS_2$-type) structure and is referred to as "CH"[16] (sometimes it is also referred to as structure "40" following Kanamori and Kakehashi[57]). The conclusion that CH is the ground state of $Au_{1-x}Pd_x$ at $x=1/2$ has also been recently reached by Curtarolo *et al.*[15] and is quite remarkable: while the CH structure has been identified as a generic possible theoretical ground state decades ago,[8] it has not been unambiguously found previously in any actual binary system. Experimentally, three binary systems have ever been suggested to have this structure: NbP,[89] ThPb, and UPb.[90] Later, NbP was found to have a different (NbAs) structure,[91] while the yet-unconfirmed assignment of ThPb and UPb to the particular space group allowed by the symmetry was done merely on the basis of plausibility of the observed c/a ratio and not by fitting the measured Bragg peak intensities. We predict AuPd to be the first binary compound not involving $5f$ elements to order in CH structure.

In a simple Ising model including only nearest- and second-nearest neighbor interactions ($J^{(1)}_{\text{pair}}$, $J^{(2)}_{\text{pair}}$), CH is a ground state[8] if (i) $J^{(1)}_{\text{pair}}>0$, (ii) $J^{(2)}_{\text{pair}}>0$, and (iii) $J^{(1)}_{\text{pair}}>J^{(2)}_{\text{pair}}/2$. Under these conditions, $\gamma 1$, $D0_{22}$, and A_5B are also ground states of the same Ising model. We find from our CE that all those latter structures are *not* ground states of Au-Pd, although they indeed have low energy and had been predicted as ground states before the outer loop converged.

E. Data mining vs cluster expansion: Evidence against the existence of non-fcc structures in Au-Pd

Recently, Curtarolo *et al.* developed[15,53] an *ab initio* data mining algorithm to search for ground states which are in

principle unrestricted by an underlying lattice. Instead, this method relies on a fixed library of N_0 candidate ground-state structures which is assembled by physical intuition, where N_0 must be small enough to be handled by routine LDA calculations. Thus, the study of Ref. 15 is complementary to ours in a way: data mining $N_0=176$ candidate structures allow for a quick but inexhaustive cross-comparison of many different underlying lattices, while we are able to focus on an in principle unrestricted space of relaxed candidate structures (in practice, $>3\times10^6$ structures) which can be derived from an fcc lattice.

The most interesting comparison is to be made at composition $x=1/3$, where both approaches predict the existence of *different* ground states of $Au_{1-x}Pd_x$: data mining predicts the non-fcc structure $C37$, while our CE predicts the two degenerate fcc-based Au_8Pd_4 structures. To compare the energies of those structures we must be very sure about LDA convergence. To do so we repeated a number of calculations of Ref. 15 *highly converged* numerical parameters[77,92] and for some structures found that our results are lower by ~10 meV. For example, for $L1_1$, Ref. 15 reports $E_{tot}=-5.463$eV/atom, while we obtain $E_{tot}=-5.475$eV/atom (using the same cutoff energy for the basis set). A similar discrepancy exists for $AuPd_3$ $L1_2$. Having established strict convergence criteria we next compute the energies of the competing structures at composition $x=1/3$. We find that $\Delta H_{LDA}(Au_8Pd_4)$ is 3 meV/atom lower than $\Delta H_{LDA}(C37)$. (Our numerical convergence allows us to clearly resolve this difference.) Moreover, we have analyzed the ratios of interatomic distances in $C37$ before and after the relaxation and concluded that upon the relaxation the interatomic environment in the relaxed $C37$ structure tends toward an fcc-like local environment. This fact and the fact that our predicted ground states are lower that all the non-fcc structures found in Ref. 15 allow us to conclude that the suggested non-fcc ground states of Au-Pd are not real.

Our own study and the data mining study[15] agree that Au_3Pd $D0_{23}$ and AuPd CH are ground states of AuPd. Most other structures predicted by our study were not within the reach of the method of Ref. 15, with one important exception: at $AuPd_3$, our $\Delta H_{LDA}(L1_2)$ is 12 meV lower than the result of Curtarolo *et al.* This discrepancy in LDA input places $L1_2$ on our ground-state line, while in Ref. 15 it was concluded that $AuPd_3$ may phase separate into AuPd CH and fcc Pd instead. Based on our convergence tests, we predict that $AuPd_3$ would not phase separate but order into $L1_2$ structure at low T. In addition, $AuPd_3L1_2$ is among those structures whose ΔH_{LDA} we have explicitly verified using the full-potential linear augmented-plane-wave (LAPW) electronic structure method (cf. Sec. III). It is thus our conviction that $AuPd_3$ $L1_2$ is a ground state of Au-Pd, at variance with the earlier conclusion of Ref. 15.

VIII. CONCLUSIONS

An objective expansion of the LDA configurational energies via multipair multi-many-body interactions was determined for the Au-Pd alloy system. This has been done by (a) selecting important many-body interactions based on LDA data for a fixed set of input structures and (b) iteratively augmenting the LDA input with structures that carry the most new information. We selected the important interactions from a large, unbiased pool of possibilities using a genetic algorithm. The interactions are found solely by their ability to predict accurately LDA energies of structures not used in the fit rather than by aesthetically appealing methods requiring the "local completeness"[70] or "physical meaning"[69,93] of the interaction set. The resulting cluster expansion shows unexpectedly long-range *pairs* (up to 13th inequivalent neighbor), as well as five *three-body* terms (with constituent pairs extending to third, fourth, sixth, and ninth neighbors), plus two *four-body* terms (with constituent pairs extending to third and fourth neighbors). This expansion requires ~50 input LDA energies and predicts a very large number of *other* LDA energies with an error of ~3 meV/atom.

Using this cluster expansion we conducted a ground-state search of ~1 500 000 possible structures finding that (i) all the ground states of Au-Pd are fcc structures; (ii) the predicted low-T-ordered states of bulk Au-Pd are different from those observed in thin films; specifically, the predicted ordered states of bulk Au_3Pd and AuPd are $D0_{23}$ and CH, respectively, whose energies are found to be lower than the (bulk) energies of the structures seen in thin films ($L1_2$ and $L1_0$, respectively) by almost 10 meV per atom; (iii) $AuPd_3$ $L1_2$ is stable and does not phase separate; (iv) at compositions around $x\sim1/4$, several one- and two-dimensional long-period superstructures are stable at low T; (v) there are a number of completely unsuspected ground states (including the structure Au_7Pd_5 with the lowest formation enthalpy), all of which could not be predicted by other theoretical methods.

We show that (a) one must vary the input structures to obtain a reliable cluster expansion, (b) data mining[15,53] misses a few important ground states obtained by the cluster expansion, and (c) previous methods based on searching a rather small library of structures[12,13,38–48,50] may miss most ground states obtained by the cluster expansion coupled to a direct enumeration ground-state search.

Note added in proof.

Recently, a paper was published by Sluiter *et al.* (SCP)[94] describing a different cluster expansion investigation of Au-Pd. While there are similarities in the results, there are also important differences which we would like to clarify for the reader.

Methodology. Like the present study, SCP also perform a cluster expansion (CE) starting from the input first-principles formation energies of various ordered Au-Pd structures and then invert this information to deduce effective interactions that are then used to survey the possible $T=0$ ground-state structures. Important differences include: (i) SCP calculate the total energies via the generalized gradient approximation (GGA) while we use the LDA. Also, SCP used the projector augmented wave (PAW) method while we use ultrasoft pseudopotentials. We have repeated the ccalculations of formation energies for a few structures using the PAW-GGA

method and find rather similar results to our ultrasoft pseudopotential (USP). For example, −80.8 meV (PAW-GGA) vs −80.5 (USP-LDA) for Au_3Pd $D0_{22}$, and respectively, −84.0 vs −83.3 meV for Au_3Pd $D0_{23}$, −97.6 vs −92.6 meV for AuPd CH, −53.8 vs −49.7 meV for $AuPd_3$ $D0_{22}$, and −55.6 vs −52.2 meV for $AuPd_3$ $L1_2$. (ii) In constructing the cluster expansion, SCP use a single, fixed set of input structures rather than expand iteratively the size of the input set, as done in the present work ("outer loop iterations"). Figure 11 in the present paper demonstrates how the omission of such "outer loop iterations" might lead to missing important ground states and to the prediction of spurious ground states. (iii) The pair and many-body interactions used by SCP are restricted to maximum the third nearest neighbor distance. As indicated in Sec. IV of the present paper, such a "level 1" set of interactions is too small to resolve the energetic order of the "long period superstructures" (LPS). The current approach uses a more extended set of interactions ("level 4" in Sec. IV). (iv) SCP construct their CE so that the inclusion of any interaction type ("cluster") deemed important triggers the automatic inclusion of all the smaller interaction types ("sub-clusters"). This burdens the CE with the need to fit a large number of interaction types, whether they are important or not. Given the limited amount of input data, this approach may have larger prediction errors, relative to what was found in our present work, as is seemingly apparent by comparing Fig. 8 of SCP with Fig. 9 in the present paper. Instead, the present work selects from a large pool of potential clusters only the important interactions using an objective criteria of minimization of prediction errors in a GA search; no *a priori* rules are established as to which interactions are automatically entitled to be included. (v) SCP search a space of $\sim 10^6$ CEs, whereas the current GA searches a larger CE space ($\sim 10^{16}$ CEs). (vi) SCP limit the ground state search to superstructures with unit vectors that are shorter than the fcc cube diagonal. This excludes six out of the eight ground states shown in our Fig. 14.

Predicted Ground States. We agree with SCP on the following issues: (i) (201) A_2B_2 superlattice (CH or "Str. 40") is the ground state at composition 50% (atomic % Pd); (ii) the ground states at 25% and 75% are structures obtained from the $L1_2$ structure by introduction of antiphase domain boundaries; (iii) there is a line of near-ground-state structures in the Au-rich region; and (iv) there are ground states between compositions 25% and 50%. The key differences are: (a) according to SCP the structure that has the lowest ΔH occurs at 50% composition while we find the global minimum formation energy to be Au_7Pd_5 at composition of 41.7%; (b) the identities of the ground states at 25% and 75% are, respectively, $D0_{23}$ and $L1_2$ in the present work and $D0_{22}$ and $D0_{22}$ in the SCP study; (c) between compositions 25% and 50%, SCP predict the Au_4Pd_2 and Au_5Pd_3 ground states while we predict the $Au_{11}Pd_4$, Au_8Pd_4, and Au_7Pd_5 ground states; (d) SCP do not predict the two-dimensional LPS ground states $Au_{13}Pd_4$ and $Au_{11}Pd_4$ found in the present work.

ACKNOWLEDGMENTS

Work at NREL was supported by U.S. DOE-SC-BES-DMS, under NREL Contract No. DEAC36-98-GO10337. Work in Universität Erlangen-Nürnberg was supported by DFG (Mu1648/3).

*Present address: Fritz-Haber Institut der Max-Planck Gesellschaft, Berlin, Germany.
†Electronic address: alex_zunger@nrel.gov

[1] A. F. Wells, *Inorganic Chemistry*, 5th ed. (Clarendon Press, Oxford, 1984).
[2] J. K. Burdett, *Chemical Bonding in Solids* (Oxford University Press, 1995).
[3] L. Darken and L. W. Gurry, *Physical Chemistry of Metals* (McGraw-Hill, New York, 1953).
[4] W. Hume-Rothery, *Atomic Theory for Students in Metallurgy* (Institute of Metals, London, 1945).
[5] J. C. Phillips, *Bonds and Bands in Semiconductors* (Academic Press, New York, 1973).
[6] A. Zunger, in NATO ASI on *Statics and Dynamics of Alloy Phase Transformations* (Plenum Press, New York, 1994), p. 361.
[7] A. Zunger, Phys. Rev. B **22**, 5839 (1980); in *Structure and Bonding in Crystals* (Academic Press, New York, 1981), Vol. 1, p. 73.
[8] F. Ducastelle, *Order And Phase Stability in Alloys* (North-Holland, Amsterdam, 1991).
[9] D. G. Pettifor, *Bonding and Structure of Molecules and Solids* (Clarendon Press, Oxford, 1995).
[10] D. de Fontaine, Solid State Phys. **47**, 33 (1994).
[11] P. Villars, in *Intermetallic Compounds, Principles and Practice*, edited by J. H. Westbrook and R. L. Fleishcer (Wiley, New York, 1995), Vol. 1, Chap. 11.
[12] S. Takizawa, K. Terakura, and T. Mohri, Phys. Rev. B **39**, 5792 (1989).
[13] Z. W. Lu, S.-H. Wei, and A. Zunger, Phys. Rev. B **44**, 10470 (1991).
[14] S. Müller and A. Zunger, Phys. Rev. Lett. **87**, 165502 (2001).
[15] S. Curtarolo, D. Morgan, and G. Ceder, CALPHAD: Comput. Coupling Phase Diagrams Thermochem. **29**, 163 (2005).
[16] L. G. Ferreira, S.-H. Wei, and A. Zunger, Phys. Rev. B **40**, 3197 (1989).
[17] R. Hultgren, P. D. Desai, D. T. Hawkins, M. Gleiser, and K. K. Kelley, *Selected Values of the Thermodynamic Properties of Binary Alloys* (American Society for Metals, Metals Park, OH, 1973).
[18] F. H. Hayes and O. Kubaschewski, Met. Sci. J. **5**, 37 (1971).
[19] At zero temperature an alloy system must either order or phase separate, but cannot be random. This is a direct consequence of the Nernst theorem, since a disordered alloy would have finite entropy.
[20] A. Nagasawa, Y. Matsuo, and J. Kakinoki, J. Phys. Soc. Jpn. **20**, 1881 (1965).
[21] Y. Matsuo, A. Nagasawa, and J. Kakinoki, J. Phys. Soc. Jpn. **21**, 2633 (1966); Y. Kawasaki, S. Ino, and S. Ogawa, *ibid.* **30**, 1758 (1971).

[22] A. Nagasawa, J. Phys. Soc. Jpn. **19**, 2344 (1964).
[23] F. K. LeGoues, V. P. Kesan, and S. S. Iyer, Phys. Rev. Lett. **64**, 40 (1990).
[24] K. L. Whiteaker, I. K. Robinson, J. E. Van Nostrand, and D. G. Cahill, Phys. Rev. B **57**, 12410 (1998).
[25] I. P. M. Bouchoms, W. A. Schoonveld, J. Vrijmoeth, and T. M. Klapwijk, Synth. Met. **104**, 175 (1999).
[26] A. Zunger and S. Mahajan, in *Handbook on Semiconductors*, edited by S. Mahajan (Elsevier, Amsterdam, 1994), Vol. 3, Chap. 19.
[27] D. de Fontaine and J. Kulik, Acta Metall. **33**, 145 (1985).
[28] Z. W. Lu, D. B. Laks, S.-H. Wei, and A. Zunger, Phys. Rev. B **50**, 6642 (1994).
[29] G. Ceder, D. de Fontaine, H. Dreysse, D. M. Nicholson, G. M. Stocks, and B. L. Gyorffy, Acta Metall. Mater. **38**, 2299 (1990).
[30] D. Broddin, G. van Tendeloo, J. Vanlanduyt, S. Amelinckx, R. Portier, M. Guymont, and A. Loiseau, Philos. Mag. A **54**, 395 (1986).
[31] D. S. hindo, K. Hiraga, T. Oikawa, and N. Mori, J. Electron Microsc. **39**, 449 (1990).
[32] G. van Tendeloo and S. Amelinckx, Phys. Status Solidi A **71**, 185 (1982).
[33] T. Nakano, A. Negishi, K. Hayashi, and Y. Umakoshi, Acta Mater. **47**, 1091 (1999).
[34] K. Hiraga, D. Shindo, and M. Hirabayashi, J. Appl. Crystallogr. **14**, 185 (1981).
[35] G. Van Tendeloo and S. Amelinckx, Phys. Rev. B **38**, 9628 (1988).
[36] For ease of comparison with $L1_2$ and $D0_{22}$, we refer to $D0_{23}$ as an Au_3Pd (or $AuPd_3$) structure, although the unit cell of $D0_{23}$ has eight (not four) inequivalent atoms.
[37] S. Müller and A. Zunger, Phys. Rev. B **63**, 094204 (2001).
[38] M. T. Yin and M. L. Cohen, Phys. Rev. Lett. **50**, 2006 (1984).
[39] S. Froyen and M. L. Cohen, Phys. Rev. B **28**, 3258 (1983); *ibid.* **29**, R3770 (1984).
[40] A. Y. Liu and M. L. Cohen, Phys. Rev. B **41**, 10727 (1990).
[41] S.-H. Wei and H. Krakauer, Phys. Rev. Lett. **55**, 1200 (1985).
[42] M. Causà, R. Dovesi, C. Pisani, and C. Roetti, Phys. Rev. B **33**, 1308 (1986); S. Limpijumnong and W. R. L. Lambrecht, *ibid.* **63**, 104103 (2001).
[43] J. W. D. Connolly and A. R. Williams, Phys. Rev. B **27**, R5169 (1983).
[44] C. Amador, W. R. L. Lambrecht, M. van Schilfgaarde, and B. Segall, Phys. Rev. B **47**, 15276 (1993).
[45] R. Kikuchi, J. M. Sanchez, D. de Fontaine, and H. Yamauchi, Acta Metall. **28**, 651 (1980).
[46] T. Mohri, S. Takizawa, and K. Terakura, Mater. Trans., JIM **31**, 315 (1990); T. Mohri, K. Terakura, S. Takizawa, and J. M. Sanchez, Acta Metall. Mater. **39**, 493 (1991).
[47] F. Ducastelle and F. Gautier, J. Phys. F: Met. Phys. **6**, 2039 (1976); P. P. Singh and A. Gonis, Phys. Rev. B **47**, 6744 (1993).
[48] A. Gonis, X.-G. Zhang, A. J. Freeman, P. Turchi, G. M. Stocks, and D. M. Nicholson, Phys. Rev. B **36**, 4630 (1987).
[49] P. Weinberger, *Electron Scattering Theory for Ordered and Disordered Matter* (Clarendon, Oxford, 1990).
[50] P. Weinberger, C. Blaas, B. I. Bennett, and A. M. Boring, Phys. Rev. B **47**, 10158 (1993).
[51] M. Sluiter, P. Turchi, Fu Zezhong, and D. de Fontaine, Phys. Rev. Lett. **60**, 716 (1988).
[52] P. E. A. Turchi, M. Sluiter, F. J. Pinski, D. D. Johnson, D. M. Nicholson, G. M. Stocks, and J. B. Staunton, Phys. Rev. Lett. **67**, 1779 (1991).
[53] S. Curtarolo, D. Morgan, K. Persson, J. Rodgers, and G. Ceder, Phys. Rev. Lett. **91**, 135503 (2003).
[54] J. Kanamori, Prog. Theor. Phys. **35**, 16 (1966).
[55] T. Kudo and S. Katsura, Prog. Theor. Phys. **56**, 435 (1976).
[56] J. M. Sanchez and D. de Fontaine, *Structure and Bonding in Crystals* (Academic Press, New York, 1981), Vol. 2, p. 117.
[57] J. Kanamori and Y. Kakehashi, J. Phys. (Paris), Colloq. **38**, C7–274 (1977).
[58] J. Kanamori, *Modulated Structures* (AIP, New York, 1979), p. 117.
[59] J. W. Cahn and R. Kikuchi, Acta Metall. **27**, 1329 (1979).
[60] L. G. Ferreira, S.-H. Wei, and A. Zunger, Int. J. Supercomput. Appl. **5**, 34 (1991).
[61] D. B. Laks, L. G. Ferreira, S. Froyen, and A. Zunger, Phys. Rev. B **46**, 12587 (1992).
[62] G. L. W. Hart, V. Blum, M. J. Walorski, and A. Zunger, Nat. Mater. **4**, 167 (2005); V. Blum, G. L. W. Hart, M. J. Walorski, and A. Zunger, Phys. Rev. B **72**, 165113 (2005).
[63] J. M. Sanchez, F. Ducastelle, and D. Gratias, Physica A **128**, 334 (1984).
[64] V. Ozoliņš, C. Wolverton, and A. Zunger, Phys. Rev. B **57**, 4816 (1998).
[65] C. Wolverton, V. Ozoliņš, and A. Zunger, J. Phys.: Condens. Matter **12**, 2749 (2000).
[66] V. Blum and A. Zunger, Phys. Rev. B **70**, 155108 (2004).
[67] J. Shao, J. Am. Stat. Assoc. **88**, 486 (1993).
[68] The pool of MBIT's used for this work consists of all three-body MBIT's involving up to ninth nearest-neighbor interactions (76 MBIT's), all four-body MBIT's involving up to fourth nearest-neighbor interactions (35 MBIT's), the single five-body and the single six-body MBIT's limited to the second nearest-neighbor interactions. Note that the entire pool provides a CE basis which is "physically meaningful" in the language of Ref. 69 or "locally complete" in the language of Ref. 70.
[69] A. van de Walle and G. Ceder, J. Phase Equilib. **23**, 348 (2002).
[70] N. A. Zarkevich and D. D. Johnson, Phys. Rev. Lett. **92**, 255702 (2005).
[71] A. van de Walle and G. Ceder, J. Phase Equilib. **23**, 349 (2002).
[72] Indeed, a frequent ground-state prediction is more likely to be confirmed by direct LDA calculation. On the other hand, in case the LDA calculation does *not* confirm a ground state predicted by *several* CE candidates, using the correct ΔH_{LDA} value in the next CE iteration step will raise the CV scores of *all* those candidates, favoring the CE candidates that make only correct predictions. This policy allows us to chose the structures for the computationally expensive LDA calculations more effectively.
[73] W. Kohn and L. J. Sham, Phys. Rev. **140**, A1133 (1965); D. M. Ceperley and B. J. Alder, Phys. Rev. Lett. **45**, 566 (1980); J. P. Perdew and A. Zunger, Phys. Rev. B **23**, 5048 (1981).
[74] P. Hohenberg and W. Kohn, Phys. Rev. **136**, B864 (1964).
[75] D. Vanderbilt, Phys. Rev. B **41**, R7892 (1990).
[76] G. Kresse and J. Furthmüller, Phys. Rev. B **54**, 11169 (1996).
[77] For routine VASP calculations, we used Monkhorst-Pack $14\times14\times14$ **k** grids, an energy cutoff of $E_{cut}=248.7$ eV, "high" precision setting [avoiding "wraparound" errors during fast Fourier transform (FFT)], evaluating the projection operators entirely in the reciprocal space and performing at least two consecutive relaxation runs to eliminate the effects of distortion of the basis set due to relaxation.

[78] P. Blaha, K. Schwarz, G. K. H. Madsen, D. Kvasnicka, and J. Luitz, WIEN2K, an augmented plane wave+local orbitals program for calculating crystal properties, Karlheinz Schwarz, Technical Universität Wien, Austria, 2001.
[79] F. D. Murnaghan, Proc. Natl. Acad. Sci. U.S.A. **30**, 244 (1944).
[80] For LAPW calculations in compounds, we used the relaxed ionic positions found by VASP.
[81] For the LPS structures in $CuPd_3$ (cf. Fig. 1), it is possible to find a "level 3" cluster expansion that keeps $D0_{23}$ at an energy higher than $L1_2$ and lower than $D0_{22}$. This will necessarily reverse the relative position of $D0_{23}$ and of the $L1_2+D0_{22}$ average, but will reproduce the energetic hierarchy of $L1_2$, $D0_{22}$, and $D0_{23}$ in both $CuPd_3$ and Cu_3Pd.
[82] Z. W. Lu, D. B. Laks, S.-H. Wei, and A. Zunger, Phys. Rev. B **50**, 6642 (1994).
[83] For the first iteration, the pool of MBIT's is restricted by using the three-body MBIT's involving only up to the fifth nearest neighbor (20 MBIT's). Pools of the four-, five- and six-body interactions are not restricted additionally.
[84] The values of t and λ were scanned from 1 to 20 and n_{pairs} from 4 to 20.
[85] The structures removed from the LDA convex hull at iteration i can be inferred from the IT=i+1 column of Fig. 11, where the LDA data include the newly calculated ΔH_{LDA} values.
[86] The many "incorrect" CE predictions in the low-x range reflect only the tight competition between the many ground-state and near-ground-state structures. Our final CE is able to reproduce even fine details of this competition, while the early iterations were quantitatively close but not always qualitatively in agreement with the LDA.
[87] M. Sanati, L. G. Wang, and A. Zunger, Phys. Rev. Lett. **90**, 045502 (2003).
[88] In fact we find that all three LPS ground states predicted by our CE can be formally described as (401) superlattices—that is, as series of (401) planes of pure Pd and pure Au.
[89] N. Schönberg, Acta Chem. Scand. (1947-1973) **8**, 226 (1954).
[90] A. Brown, Acta Crystallogr. **14**, 856 (1961).
[91] H. Boller and E. Parthé, Acta Crystallogr. **16**, 1095 (1963).
[92] A possible source of disagreement with Ref. 15 is that, according to the data available at http://datamine.mit.edu, the calculations of Ref. 15 were performed with "medium" precision (allowing for the "wraparound" errors) and somewhat smaller **k** grids.
[93] M. H. F. Sluiter and Y. Kawazoe, Phys. Rev. B **71**, 212201 (2005).
[94] M. H. F. Sluiter, C. Colinet, and A. Pasturel, Phys. Rev. B **73**, 174204 (2006).